INFORMATION TO USERS

This manuscript has been reproduced from the microfilm master. UMI films the text directly from the original or copy submitted. Thus, some thesis and dissertation copies are in typewriter face, while others may be from any type of computer printer.

The quality of this reproduction is dependent upon the quality of the copy submitted. Broken or indistinct print, colored or poor quality illustrations and photographs, print bleedthrough, substandard margins, and improper alignment can adversely affect reproduction.

In the unlikely event that the author did not send UMI a complete manuscript and there are missing pages, these will be noted. Also, if unauthorized copyright material had to be removed, a note will indicate the deletion.

Oversize materials (e.g., maps, drawings, charts) are reproduced by sectioning the original, beginning at the upper left-hand corner and continuing from left to right in equal sections with small overlaps.

Photographs included in the original manuscript have been reproduced xerographically in this copy. Higher quality 6" x 9" black and white photographic prints are available for any photographs or illustrations appearing in this copy for an additional charge. Contact UMI directly to order.

Bell & Howell Information and Learning
300 North Zeeb Road, Ann Arbor, MI 48106-1346 USA
800-521-0600

UMI®

Properties of steady-state field in micromaser pumped by atoms in superposition of their upper and lower states

Jozef Škvarček

A dissertation submitted to the Graduate Faculty in Physics in partial fulfillment of the requirements for the degree of Doctor of Philosophy. The City University of New York

2000

Approval page

This manuscript has been read and accepted for the Graduate Faculty in Physics in satisfaction of the dissertation requirement for the degree of Doctor of Philosophy.

1/25/00
Date

Mark Hillery
Prof. Mark Hillery
Chair of Examining Committee

2/9/00
Date

Prof. Louis S. Celenza
Executive Officer

Supervisory Committee:

Prof. János Bergou
Prof. Ying-Chih Chen
Prof. Steven Greenbaum
Prof. Alexander Lisyansky

The City University of New York

Abstract

PROPERTIES OF STEADY-STATE FIELD IN MICROMASER
PUMPED BY ATOMS IN SUPERPOSITION
OF THEIR UPPER AND LOWER STATES

by

Jozef Škvarček

Advisor: Professor Mark Hillery

We present a semiclassical method for determining the phase distribution and the average photon number of a steady-state micromaser field pumped by a stream of resonant two-level atoms in a superposition of their upper and lower states. Assuming the field to have a photon number distribution with a single sharp peak, we find an equation for the amplitude and the phase of the steady-state field which has two solutions. The stability analysis shows which one of the two is physically realizable. Using the very simple time evolution of particular atomic states, valid in the semiclassical limit, we find an expression for the phase distribution of the field which contains the mean photon number as a parameter. That can be determined from the stable solution. Then we give a simple explanation for period-2 oscillations of the

electric field in a lossless, regularly-pumped micromaser with injected atomic coherence in terms of tangent and cotangent states. We also examine the effect of cavity damping on this steady state. Then we consider micromaser fields which after interaction with one atom produce disentangled atom-field states. We find a special solution for which interaction with the atom has the effect of flipping the sign of the electric field. We also consider the general case and derive conditions which the field must satisfy.

Acknowledgments

I wish to express my deep gratitude to my advisor Prof. Mark Hillery for many stimulating discussions and help when deciding on an interesting research projects. I would like to thank to Prof. János Bergou for valuable ideas on particular problems I encountered. My thanks also belong to my colleagues and friends, here I want to mention István Németh and Yonatan Abranyos, for creating friendly atmosphere. The results from the most intensive numerical calculations presented here were made possible only because of the understanding of full time faculty, I would like to mention especially Prof. Marten denBoer, who allocated funds for building our parallel cluster. Partial funding for the software was provided by the Research Foundation of the City University of New York.

Contents

List of Tables

List of Figures

Chapter 1

Introduction

A micromaser is very simple physical system which consists of a beam of two-level atoms and a single-mode electromagnetic field within a microwave cavity. Despite its simplicity and the fact that it has been the object of vigorous research for more than a decade, it still presents a researcher with new challenges.

Filipowicz et.al. in 1986 published some of the first papers on the theory of the microscopic maser [1, 2]. They investigated the steady-state cavity field and they found that as the pump rate increased, it goes through thresholds that resemble first-order phase transitions [3]. Guzman et.al. worked out the semiclassical theory, and they found that the system at a thresh-

old undergoes a transition from one branch of the semiclassical solution to the next [4]. Progress was made not only in the theoretical understanding of the system, but also, around the same time, advances in experimental physics made it possible to build superconducting high-Q microcavities, so that the field could maintain large average photon number, which combined with Rydberg-state spectroscopy, made real micromaser experiments possible. Experiments conducted at the Max Planck Institute for Quantum Optics in Garching have confirmed theoretical predictions of such quantum phenomena as sub-Poissonian photon statistics, quantum Rabi oscillations and quantum collapses and revivals [5, 6, 7, 8].

Most of the studies of the dynamics of the micromaser have considered only injected atoms in their upper states, while the situation in which the atoms enter the cavity in a coherent superposition of their upper and lower states has received far less attention. The micromaser with injected atomic coherence has been investigated by several authors. Krause et.al., assuming weak atom-field coupling, found that the phase of the atomic coherence is transferred to the micromaser field and that the excitation probability of the atoms leaving the microwave cavity depends on the relative phase angle between incoming atom dipoles and the field [9]. Since the outgoing atoms are

available for measurement, an experiment could be set up to determine the coherence of the field. Slosser et.al. studied lossless micromaser with coherent pumping and they found that the field evolves towards pure states which were named tangent and cotangent states [10, 11, 12]. These states rely on the existence of trapping states, and apart from having other non-classical properties, they can be used for generating macroscopic quantum superpositions. The authors also numerically investigated the situation when the state of the field consists of a tangent state and a cotangent state in adjacent blocks of number states. This leads to the occurrence of interesting period-2 oscillations when the steady state field returns to its initial value not after interaction with one, but after two atoms. The effect of the atomic phase was also studied for a multimode laser system; Kien et.al. developed the quantum theory of the two-mode Λ laser with atoms injected in a superposition of their states [13].

The case in which the atoms are in a coherent superposition is a more complicated problem than the case in which they are completely inverted. In the latter case, the diagonal elements of the density matrix couple only to each other, but when there is atomic coherence this is no longer the case. The entire density matrix must be treated at once. At the same time this is

also a more interesting problem since the atomic dipoles have a phase, and because they drive the field, the field has a phase as well. The steady-state field produced by atoms in their upper states has no mean phase, because any value of the phase is equally likely.

In the following chapters we would like to investigate such a micromaser with injected atomic coherence. We will present a semiclassical method for determining the average photon number, phase and the phase distribution of a steady-state micromaser field in Chapter 3. We will find that the method provides results that are in very good correspondence with numerical simulations. We will show in Chapter 4 a simple physical explanation of the period-2 oscillations of the steady-state field which will be based on the properties of the cotangent and tangent states. Then we will turn our attention to disentanglement-preserving states in micromaser in Chapter 5. We will present a general method for determining such initial field states which after interaction with one atom produce a state which is again a product of the atomic and field components. It will be shown that the cotangent and tangent states are special examples of such fields.

Chapter 2

Micromaser

A micromaser consists of a beam of two-level atoms passing through a high-Q microwave cavity containing an electromagnetic field. It is assumed that the atomic beam is of low density, i.e. at any given time there is at most one atom present in the cavity. We also assume that the microcavity supports only one mode of the field which is in resonance with the atoms at the frequency ω and that the atoms have all the same velocity, so that they pass through the cavity in a constant time τ. The atom-field interaction is governed by the Jaynes-Cummings Hamiltonian, and when the cavity is empty, the field decays into the environment. If the probability of the atoms being in their upper states is high when they enter the microcavity, then the micromaser

can maintain a non-zero steady state field.

2.1 Jaynes-Cummings model

Jaynes-Cummings model describes a single mode field coupled to a two-level atom. The atom has states $|a\rangle$, with energy ω (we are using units with $\hbar = 1$), and $|b\rangle$, with energy 0. The Hamiltonian, in the rotating-wave approximation, describing the atom-field system is

$$H = \omega a^\dagger a + \frac{1}{2}\omega(\sigma_3 + I) + g(a^\dagger \sigma^- + a\sigma^+), \tag{2.1}$$

where a, $a^\dagger$ are the annihilation and creation Bose operators for the field obeying the standard commutation relations

$$[a^\dagger, a] = 1, [a, a] = [a^\dagger, a^\dagger] = 0, \tag{2.2}$$

σ_3 and $\sigma^\pm$ are the Pauli spin operators, and g is the atom-field interaction constant. H acts on Hilbert space $\mathcal{H} = \mathcal{H}_{\text{atom}} \otimes \mathcal{H}_{\text{field}}$, where $\mathcal{H}_{\text{atom}}$ is two-dimensional space of physical atom states and $\mathcal{H}_{\text{field}}$ is infinite dimensional space of physical field states. The first two terms on the right hand side

of Eq. (2.1) describe free field and free atom respectively, while the third is the atom-field interaction. $\mathcal{H}_{\text{atom}}$ is spanned by the two basis vectors $|a\rangle$, $|b\rangle$, while $\mathcal{H}_{\text{field}}$ is spanned by the usual number state basis $|0\rangle$, $|1\rangle$, ... A vector from $\mathcal{H}$ then can be given as $|a,n\rangle$, $|b,n\rangle$ etc. σ^+ is the raising atomic operator acting in $\mathcal{H}_{\text{atom}}$ as follows

$$\sigma^+|b\rangle = |a\rangle, \tag{2.3}$$

$$\sigma^+|a\rangle = 0, \tag{2.4}$$

and σ^- is the lowering atomic operator

$$\sigma^-|a\rangle = |b\rangle, \tag{2.5}$$

$$\sigma^-|b\rangle = 0. \tag{2.6}$$

Operators a, $a^\dagger$ act on vectors in $\mathcal{H}_{\text{field}}$ in the following way:

$$a^\dagger|n\rangle = \sqrt{n+1}|n+1\rangle, \tag{2.7}$$

$$a|n\rangle = \sqrt{n}|n-1\rangle, \tag{2.8}$$

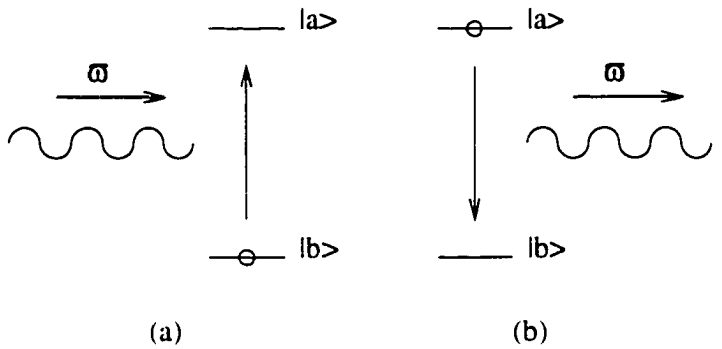

Figure 2.1: Interaction between two-level resonant atom and single-mode cavity field with frequency ω as described by the Jaynes-Cummings Hamiltonian. Part (a) shows the action of $a\sigma^+$ operator, while (b) shows the action of $a^\dagger\sigma^-$ operator.

$$a|0\rangle = 0. \tag{2.9}$$

The $a\sigma^+$ term in Eq. (2.1) describes a process when the atom makes a transition from its lower to its upper level while absorbing one photon of energy ω. Figure 2.1(a). The $a^\dagger\sigma^-$ term describes the reverse action, when one photon is emitted by the atom which goes to its ground state. Figure 2.1(b). In other words, these two terms give the transition between $|a, n\rangle$ and $|b, n+1\rangle$ states. These states form two-dimensional subspace $\mathcal{H}^{(n+1)}$ of $\mathcal{H}$, however, they are not eigenvectors of Eq. (2.1). In order to find the eigenvectors and eigenvalues, $\mathcal{H}$ is diagonalized in the space $\mathcal{H}^{(n+1)}$. By this method we find

$$E_+^{n+1} = \omega(n+1) + g\sqrt{n+1}, \tag{2.10}$$

$$E_{-}^{n+1} = \omega(n+1) - g\sqrt{n+1}, \tag{2.11}$$

as the energy spectrum and

$$|\Psi_{+}^{n+1}\rangle = \frac{1}{\sqrt{2}}(|a,n\rangle + |b,n+1\rangle), \tag{2.12}$$

$$|\Psi_{-}^{n+1}\rangle = \frac{1}{\sqrt{2}}(|a,n\rangle - |b,n+1\rangle), \tag{2.13}$$

as the eigenvectors of H on subspace $\mathcal{H}^{(n+1)}$. States $|a,n\rangle$ and $|b,n+1\rangle$ may be expressed via $|\Psi_{+}^{n+1}\rangle$ and $|\Psi_{-}^{n+1}\rangle$ and then their time evolution can be found in the interaction picture in terms of the map

$$|a,n\rangle \rightarrow \left\{\cos(g\tau\sqrt{n+1})|a,n\rangle - \mathrm{i}\sin(g\tau\sqrt{n+1})|b,n+1\rangle\right\}. \tag{2.14}$$

$$|b,n+1\rangle \rightarrow \left\{\cos(g\tau\sqrt{n+1})|b,n+1\rangle - \mathrm{i}\sin(g\tau\sqrt{n+1})|a,n\rangle\right\}. \tag{2.15}$$

If the atom is initially in the state

$$|\Psi_{\mathrm{at}}\rangle = \alpha|a\rangle + \beta|b\rangle, \tag{2.16}$$

where α and β are complex numbers satisfying the normalization condition $|\alpha|^2 + |\beta|^2 = 1$, and the field is initially in the state

$$|f\rangle = \sum_{n=0}^{\infty} d_n |n\rangle, \tag{2.17}$$

then after a time τ the state of the combined system will be

$$\begin{aligned} |f\rangle \otimes (\alpha|a\rangle + \beta|b\rangle) \quad \rightarrow \quad & \sum_{n=0}^{\infty} d_n (\alpha c_{n+1} |n\rangle - \mathrm{i}\beta s_n |n-1\rangle) \otimes |a\rangle \\ & + \sum_{n=0}^{\infty} d_n (\beta c_n |n\rangle - \mathrm{i}\alpha s_{n+1} |n+1\rangle) \otimes |b\rangle. \end{aligned} \tag{2.18}$$

where

$$s_n = \sin(g\tau\sqrt{n}) = \sin(\theta_{\mathrm{int}}\sqrt{n/N_{\mathrm{ex}}}) \tag{2.19}$$

$$c_n = \cos(g\tau\sqrt{n}) = \cos(\theta_{\mathrm{int}}\sqrt{n/N_{\mathrm{ex}}}). \tag{2.20}$$

Here, we have introduced the pumping parameter $\theta_{\mathrm{int}} = \sqrt{N_{\mathrm{ex}}} g\tau$. The number N_{ex} is the mean number of atoms interacting with the cavity field during its lifetime. Eq. (2.18), which is written in the interaction picture defines the Jaynes-Cummings time evolution of the field density matrix $\hat{\rho} = \mathrm{Tr}_{\mathrm{at}} \hat{\rho}_{\mathrm{system}}$ which can be written formally as $\hat{\rho}(\tau) = M\hat{\rho}(0)$, and in the number-state

representation we have

$$\begin{aligned}
\rho_{nm} \rightarrow\ & \rho_{nm}(|\alpha|^2 c_{n+1}c_{m+1} + |\beta|^2 c_n c_m) \\
& + \rho_{n-1,m-1}|\alpha|^2 s_n s_m \\
& + \rho_{n+1,m+1}|\beta|^2 s_{n+1}s_{m+1} \\
& + i\alpha\beta^*(c_{n+1}s_{m+1}\rho_{n,m+1} - s_n c_m \rho_{n-1,m}) \\
& + i\alpha^*\beta(c_n s_m \rho_{n,m-1} - s_{n+1}c_{m+1}\rho_{n+1,m}),
\end{aligned} \tag{2.21}$$

where $\rho_{nm} = \langle n|\hat{\rho}|m\rangle$. As one can see, the interaction couples together elements from different diagonals which makes its analysis complicated. In the case of non-coherent pumping, $|\alpha\beta| = 0$, only the diagonal terms are coupled, Figure 2.2.

2.2 Master equation

The cavity field decays into the environment during the time interval when the cavity is empty. The losses during the atom-field interaction are neglected since the interaction time is much shorter. If we want to develop a correct physical model for the loss process we must proceed carefully. An

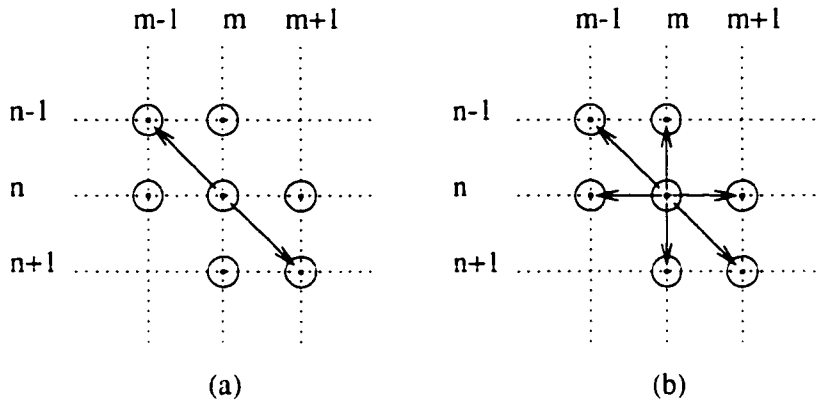

Figure 2.2: Coupling among field density matrix elements as given by Eq. (2.21). If pumping atoms are not in the coherent superposition, $|\alpha\beta| = 0$, then only elements at the same diagonal are coupled together, part (a). Otherwise, the interaction couples also elements from neighboring diagonals, part (b).

attempt to describe damping of the quantized single mode micromaser field phenomenologically by an analogy with classical physics leads to commutation relations for the field operators that violate the uncertainty principle. In order to preserve the correct commutation relations we need a quantum noise generator which has sufficient output at zero temperature.

We may model the cavity losses by assuming a stream of a large number of two-level atoms, that have high probability being at their lower level, interacting with the cavity field. We look at these atoms as at a reservoir (the environment) which is in contact with our system, the cavity field. The

total Hamiltonian H_T, which has the form of Eq. (2.1), can be expressed

$$H_T = H_{field} + H_{res} + V, \tag{2.22}$$

where $H_0 = H_{field} + H_{res}$ is the free part and V describes the interaction. The reservoir is weakly coupled to the field which loses its energy to it. We also suppose that the fluctuations in the reservoir couple back into the field. However, the reservoir has such properties that prevent the excitation energy, initially in the field, from returning completely from the reservoir.

The statistical properties of the total system are given by total density operator $\hat{\rho}(t)$ which satisfies equation of motion

$$i\hbar\frac{\partial\hat{\rho}}{\partial t} = [H_0 + V, \hat{\rho}]. \tag{2.23}$$

We are interested in the properties of the field only, therefore, our objective is to find an equation of motion for the reduced field density operator $\hat{\rho}_{field}(t) = \mathrm{Tr}_{res}\hat{\rho}$. First, we transform Eq. (2.23) into the interaction picture to remove rapidly varying system motion. Then we trace the equation with respect to the reservoir's degrees of freedom. The resulting equation can be formally integrated for the field density matrix in the interaction picture with the help

of the perturbation theory, since the atom-field coupling is weak, keeping terms up to the second order of V. Then we need to make the Markov approximation by assuming that the reservoir correlation time is zero on a time scale in which the cavity field loses an appreciable amount of its energy. The Markov approximation in our case means that the future of the field depends on present only. This assumption is sufficient to ensure that the reservoir behaves according our conditions, that is, the excitation energy can not return back from the reservoir.

After all of the work we find that the decay of the micromaser field during the time interval when the cavity is empty, formally given as $\hat{\rho}(t) = \mathrm{e}^{Lt}\hat{\rho}(0)$ (subscript *field* was omitted), is described by the master equation [14]

$$\begin{aligned}\frac{\mathrm{d}\hat{\rho}}{\mathrm{d}t} = L\hat{\rho} &= -\frac{1}{2}\gamma(n_{\mathrm{b}}+1)(a^{\dagger}a\hat{\rho}+\hat{\rho}a^{\dagger}a-2a\hat{\rho}a^{\dagger}) \\ &\quad -\frac{1}{2}\gamma n_{\mathrm{b}}(aa^{\dagger}\hat{\rho}+\hat{\rho}aa^{\dagger}-2a^{\dagger}\hat{\rho}a),\end{aligned} \tag{2.24}$$

where n_{b} is the mean photon number in the thermal background and γ is the loss coefficient. Its reciprocal $1/\gamma$ is equal to the mean cavity lifetime. We will consider the case when the environment the micromaser cavity is in

contact with is at zero temperature. That implies $n_b = 0$ and

$$\frac{d\hat{\rho}}{dt} = L\hat{\rho} = -\frac{1}{2}\gamma(a^\dagger a\hat{\rho} + \hat{\rho}a^\dagger a - 2a\hat{\rho}a^\dagger), \tag{2.25}$$

which has the solution in the number-state representation

$$\rho_{mn}(t) = e^{-\gamma t(m+n)/2}\sum_{l=0}^{\infty}\left(\frac{(m+l)!}{m!}\frac{(n+l)!}{n!}\right)^{1/2}\frac{(1-e^{-\gamma t})^l}{l!}\rho_{m+l,n+l}(0). \tag{2.26}$$

The times at which the pumping atoms are injected into the microwave cavity may conform to various distributions. For the case when they obey Poissonian statistics we can derive the equation of motion for the average field density matrix in the form of a master equation [1]

$$\frac{d\hat{\rho}}{dt} = r(M-1)\hat{\rho} + L\hat{\rho}. \tag{2.27}$$

where r denotes the mean rate the atoms arrive at the cavity, and it is related to N_{ex} by $N_{ex} = r/\gamma$. Eq. (2.27) can be employed for finding the steady-state field density matrix by putting $d\hat{\rho}/dt = 0$. On the other hand when considering a regularly pumped micromaser, i.e. when the time T between two consecutive atoms is constant, the time evolution of the field

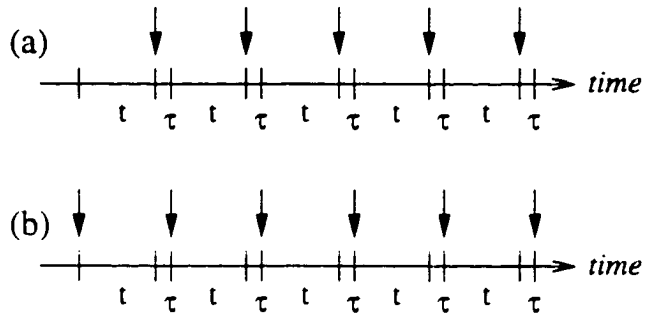

Figure 2.3: The time scale for the regularly pumped micromaser. The atom-field interaction time τ is much smaller then the time interval between two consecutive atoms t. The field can be measured just before the next atom enters the cavity, the arrows in (a), or just after the interaction (b), for example.

density matrix is given by the map

$$\hat{\rho}(t_{i+1}) = \mathrm{e}^{LT} M \hat{\rho}(t_i), \tag{2.28}$$

if t_i are the times the atoms enter the cavity, $t_{i+1} - t_i = T$. The steady state is usually defined for this case as $\hat{\rho}(t_{i+1}) = \hat{\rho}(t_i) = \rho_{\mathrm{ss}}$, which says that the field density matrix is the same at any of the times just before an atom enters the cavity, see Figure 2.3(a). Of course, the density matrix could be different if measured not at t_i's; we would have different ρ_{ss} should we measure the cavity field at the times just after the atom-field interaction, for example (see Figure 2.3(b)).

It is possible to study the micromasers whose pumping statistics lie some-

where between the regular and Poissonian too [15, 16], but such cases will not be considered here.

Chapter 3

Semiclassical approximation

3.1 Introduction

Here we want to extend the semiclassical approximation, done by Guzman et.al. [4], to the micromaser with injected atomic coherence. In particular, our objective is to determine mean photon number and the phase distribution of the steady-state field. We find an equation for the amplitude and the phase of the steady-state field in Section 3.2, which can be solved and has two solutions. In order to determine which one is physically realizable, we perform a stability analysis in Section 3.3. Then we turn our attention to the problem of finding an approximate expression for the phase distribution of

the field in Section 3.4. We employ techniques developed by Gea-Banacloche to treat the problem [17]. These rely on the very simple time evolution of particular atomic states. We are able to use them to find an expression for the phase distribution which contains the mean photon number as a parameter. Our analytical results are compared to quantum-mechanical numerical simulations in Section 3.5, and we find that the agreement is very good.

3.2 Phase and amplitude of steady-state field

The objective in this section is to find the equation of motion for the amplitude and the phase of the micromaser field which will later enable us to determine the steady state values of these quantities. We will assume that the atomic pumping statistics is Poissonian. We will also assume that the steady state field has a large amplitude, and that its photon number distribution is sharply peaked around $\bar{n}$. We express the expectation value of the field annihilation operator $\langle a \rangle$ in terms of its amplitude u and phase θ

$$\langle a \rangle = u e^{i\theta}, \tag{3.1}$$

and, because of our assumptions, $\bar{n} = u^2$.

Using the standard formula for determining the mean value of an operator A, $\langle A\rangle = \mathrm{Tr}\{A\hat{\rho}\}$, and the Eq. (2.27) we are able to obtain the needed equation for $\langle a\rangle$. Firstly, we multiply Eq. (2.27) by a and then we take the trace with respect to the photon number states. On the left hand side we then get

$$\mathrm{Tr}\{a\frac{\mathrm{d}\hat{\rho}}{\mathrm{d}t}\} = \frac{\mathrm{d}}{\mathrm{d}t}\mathrm{Tr}\{a\hat{\rho}\} = \frac{\mathrm{d}}{\mathrm{d}t}\langle a\rangle, \tag{3.2}$$

since in the Shrödinger picture the operator a does not depend on time. It is easy to resolve the loss term on the right hand side of Eq. (2.27) employing the cyclic property of the trace

$$\langle aL\rangle = \frac{1}{2}\gamma\mathrm{Tr}\{[a^{\dagger}, a]a\hat{\rho}\} = -\frac{\gamma}{2}\langle a\rangle, \tag{3.3}$$

if Eq. (2.25) is considered, while proceeding with the first term is a little bit more involved. The term

$$\mathrm{Tr}\{a(M-1)\hat{\rho}\} = \langle a(M-1)\rangle \tag{3.4}$$

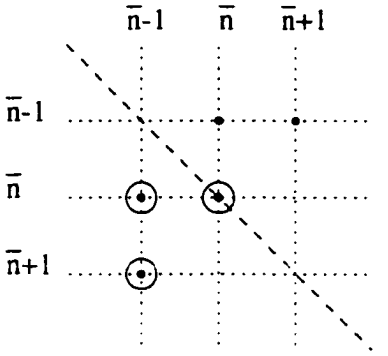

Figure 3.1: Relevant part of the field density matrix assumed in the semiclassical treatment. The dashed line represents the main diagonal, the field is strongly peaked around $\rho_{\bar{n}\bar{n}}$. In order to determine $\langle a \rangle$ also $\rho_{\bar{n},\bar{n}-1}$ and $\rho_{\bar{n}+1,\bar{n}-1}$ are needed, other elements are neglected.

can be expressed in the form

$$\begin{aligned}\langle a(M-1)\rangle = \sum_{n=0}^{\infty} \sqrt{n+1}\Big\{ & \rho_{n+1,n}(|\alpha|^2 c_{n+2}c_{n+1} + |\beta|^2 c_{n+1}c_n - 1) + \\ & \rho_{n,n-1}|\alpha|^2 s_{n+1}s_n + \rho_{n+2,n+1}|\beta|^2 s_{n+2}s_{n+1} + \\ & i\alpha\beta^*(c_{n+2}s_{n+1}\rho_{n+1,n+1} - s_{n+1}c_n\rho_{nn}) + \\ & i\alpha^*\beta(c_{n+1}s_n\rho_{n+1,n-1} - s_{n+2}c_{n+1}\rho_{n+2,n})\Big\}. \end{aligned} \tag{3.5}$$

Eq. (3.5) can be further approximated by taking into account the fact that we deal with a field whose number distribution is sharply peaked at $\bar{n}$, where $\bar{n} \gg 1$. Namely, we restrict our attention to field density matrices, which have only a few non-zero elements: $\rho_{\bar{n}\bar{n}}$ and those nearby, Figure 3.1. Then

in the sum in Eq. (3.5) only those terms will contribute that include the density matrix elements $\rho_{n_1 n_2}$, where n_1 and n_2 are close to $\bar{n}$. We also use the Taylor expansion with respect to n, keeping only terms up to the order of $1/\sqrt{\bar{n}}$, to evaluate s_{n+1} and c_{n+1} in terms of s_n and c_n, respectively. For s_{n+1} and c_{n+1} we then get

$$s_{n+1} \approx s_n + \frac{\mathrm{d}s_n}{\mathrm{d}n}, \tag{3.6}$$

$$c_{n+1} \approx c_n + \frac{\mathrm{d}c_n}{\mathrm{d}n}, \tag{3.7}$$

the derivatives of s_n and c_n can be found with the help of Eqs. (2.19) and (2.20), $\mathrm{d}s_n/\mathrm{d}n = \theta_{\mathrm{int}} c_n / 2\sqrt{n N_{\mathrm{ex}}}$ and $\mathrm{d}c_n/\mathrm{d}n = -\theta_{\mathrm{int}} s_n / 2\sqrt{n N_{\mathrm{ex}}}$ resp. Finally, if we put together what we have, we get

$$\begin{aligned} \frac{\mathrm{d}\langle a \rangle}{\mathrm{d}t} &= r \sum_{n=0}^{\infty} \left\{ \frac{1}{2\sqrt{n}} (|\alpha|^2 - |\beta|^2) s_n^2 \rho_{n,n-1} + \right. \\ &\quad \mathrm{i}\alpha\beta^* \left(-\frac{\theta_{\mathrm{int}}}{2\sqrt{N_{\mathrm{ex}}}} - \frac{s_n c_n}{2\sqrt{n}} \right) \rho_{nn} - \\ &\quad \left. \mathrm{i}\alpha^*\beta \left(\frac{\theta_{\mathrm{int}}}{2\sqrt{N_{\mathrm{ex}}}} - \frac{s_n c_n}{2\sqrt{n}} \right) \rho_{n+1,n-1} \right\} - \frac{\gamma}{2} \langle a \rangle. \end{aligned} \tag{3.8}$$

We expect the steady state micromaser field to be close to a coherent state $|\eta\rangle$, where $\eta = \langle a \rangle$ and $|\eta|^2 = \bar{n}$, which has the density matrix in the number-

state representation

$$\rho_{mn} = \mathrm{e}^{-|\eta|^2} \frac{(\eta^*)^n \eta^m}{\sqrt{m!n!}}. \tag{3.9}$$

Therefore, the non-diagonal density matrix elements in Eq. (3.8) can be expressed as

$$\frac{\eta^*}{\sqrt{n}} \rho_{n,n-1} = \rho_{nn} \tag{3.10}$$

and

$$\rho_{n+1,n-1} = \frac{\eta}{\sqrt{n+1}} \frac{\sqrt{n}}{\eta^*} \rho_{nn}. \tag{3.11}$$

Keeping in mind that ρ_{nn} is sharply peaked about $\bar{n}$, this implies that Eq. (3.8) can be put into the form

$$\begin{aligned} \frac{\mathrm{d}(u\mathrm{e}^{\mathrm{i}\theta})}{\mathrm{d}t'} &= \mathcal{N}_{\mathrm{ex}} \left\{ \frac{1}{2u}(|\alpha|^2 - |\beta|^2) s_{\bar{n}}^2 \mathrm{e}^{\mathrm{i}\theta} + \right. \\ &\quad |\alpha\beta| \mathrm{e}^{\mathrm{i}\phi} \left(-\frac{\theta_{\mathrm{int}}}{2\sqrt{N_{\mathrm{ex}}}} - \frac{s_{\bar{n}} c_{\bar{n}}}{2u} \right) - \\ &\quad \left. |\alpha\beta| \mathrm{e}^{-\mathrm{i}\phi} \left(-\frac{\theta_{\mathrm{int}}}{2\sqrt{N_{\mathrm{ex}}}} + \frac{s_{\bar{n}} c_{\bar{n}}}{2u} \right) \mathrm{e}^{2\mathrm{i}\theta} \right\} - \frac{1}{2} u \mathrm{e}^{\mathrm{i}\theta}. \end{aligned} \tag{3.12}$$

We have defined a new time parameter $t' = \gamma t$, and set

$$\mathrm{i}\alpha\beta^* = |\alpha\beta| \mathrm{e}^{\mathrm{i}\phi}. \tag{3.13}$$

Eq. (3.12) can now be solved for the two real variables u and θ. The steady-state values of u and θ are determined by setting the time derivative equal to zero. For the phase θ of the steady-state field, two solutions are possible as one can easily verify: $\theta = \phi$ and $\theta = \phi + \pi$. However, as long as we are in the classical regime, we expect that only one is physical. We will resort to a stability analysis to determine which one is stable, i.e. physically realizable, and which one is merely formal.

3.3 Stability analysis

As it was said in the previous section, Eq. (3.12) can be solved for the steady state values of $\bar{n} = u^2$ and θ. Using either solution of the phase θ we will get a transcendental equation for the mean photon number $\bar{n} = \bar{n}(\theta_{\text{int}})$ as a function of the pumping parameter θ_{int}. In order to determine whether the solution is stable we will displace the system from its steady state by $\delta\theta$ and δu, $\delta\theta \ll \theta$ and $\delta u \ll u$ respectively. If the system shows a tendency to move towards its steady state in both variables (in abstract sense the system is moving in the (u, θ) plane), the solution is stable, and vice versa.

3.3.1 Unstable solution

Let us first examine the case

$$\theta = \phi. \tag{3.14}$$

This is substituted into Eq. (3.12) which gives us the equation for $\bar{n}(\theta_{\rm int})$ at steady state,

$$0 = (|\alpha|^2 - |\beta|^2)s_{\bar{n}}^2 - 2|\alpha\beta|s_{\bar{n}}c_{\bar{n}} - \frac{\bar{n}}{N_{\rm ex}}. \tag{3.15}$$

In order to find the stable points, we change $\theta \to \theta + \delta\theta$ and $u \to u + \delta u$ in Eq. (3.12). We then employ a Taylor expansion to find both sides up to first order in $\delta\theta$ and δu. We obtain the expression for the time derivative of δu from the real part of the resulting equation,

$$\delta\dot{u} = \left\{ \frac{\theta_{\rm int}\sqrt{N_{\rm ex}}}{u}[(|\alpha|^2 - |\beta|^2)c_{\bar{n}}s_{\bar{n}} + |\alpha\beta|(s_{\bar{n}}^2 - c_{\bar{n}}^2)] - 1 \right\} \delta u \tag{3.16}$$

while from the imaginary part we have

$$\delta\dot{\theta} = |\alpha\beta|\frac{\theta_{\rm int}\sqrt{N_{\rm ex}}}{u}\delta\theta. \tag{3.17}$$

All terms on the right hand side of the last equation are positive real numbers, so that they form a positive factor multiplying $\delta\theta$. Then $\dot{\delta\theta}$ (we may say it

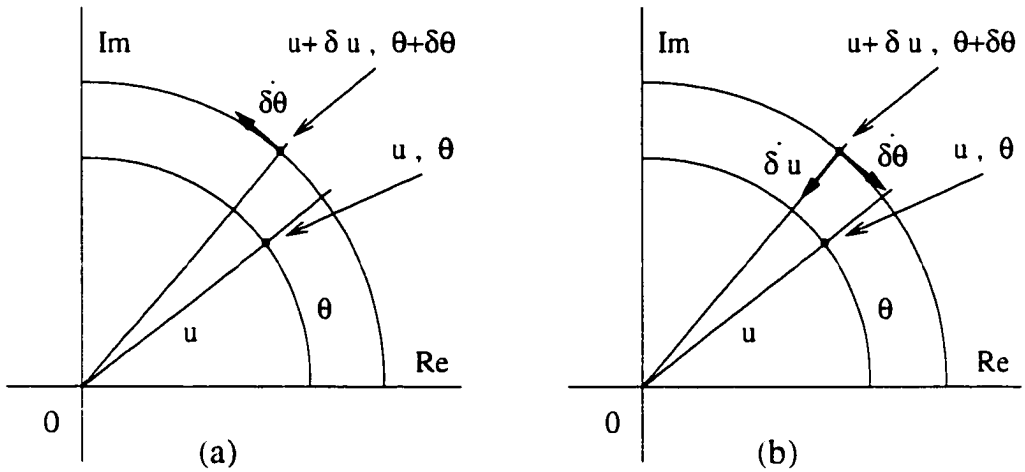

Figure 3.2: Solutions of Eq. (3.12) for the complex amplitude $\eta = ue^{i\theta}$ are represented via polar coordinates u, θ. (a) shows non-stable case for $\theta = \phi$. the "velocity" $\dot{\delta\theta}$ has the same direction as the displacement $\delta\theta$. (b) shows stable points (u,θ) for the situation when $\theta = \phi + \pi$ since both $\dot{\delta u}$ and $\dot{\delta\theta}$ at point $(u + \delta u, \theta + \delta\theta)$ point back towards (u,θ).

is the "velocity" of $\delta\theta$) always has the same direction as $\delta\theta$. That means the phase of the system at the point $(u + \delta u, \theta + \delta\theta)$ is moving away from θ, see Figure 3.2(a). Therefore, all points (u, θ) which we obtain from Eq. (3.15) are not stable.

3.3.2 Stable solution

If we repeat the procedure for

$$\theta = \phi + \pi \tag{3.18}$$

then we find

$$0 = (|\alpha|^2 - |\beta|^2)s_{\bar{n}}^2 + 2|\alpha\beta|s_{\bar{n}}c_{\bar{n}} - \frac{\bar{n}}{N_{ex}} \tag{3.19}$$

as the equation for $\bar{n}(\theta_{int})$, and, for the equations of motion for δu and $\delta\theta$.

$$\delta\dot{u} = \left\{\frac{\theta_{int}\sqrt{N_{ex}}}{u}[(|\alpha|^2 - |\beta|^2)c_{\bar{n}}s_{\bar{n}} - |\alpha\beta|(s_{\bar{n}}^2 - c_{\bar{n}}^2)] - 1\right\}\delta u \tag{3.20}$$

$$\delta\dot{\theta} = -|\alpha\beta|\frac{\theta_{int}\sqrt{N_{ex}}}{u}\delta\theta. \tag{3.21}$$

As one can see, the factor multiplying $\delta\theta$ in Eq. (3.21) has a negative sign. Therefore, the system has tendency to move from the state with phase $\theta + \delta\theta$ back to θ. However, we still have to check the behavior of $\dot{\delta u}$ in order to determine whether the point (u, θ) is stable. It is hard to see by inspection of Eq. (3.20) what the direction of $\dot{\delta u}$ is. We need the term in the curly brackets to be negative for the field to be at stable (u, θ), see Figure 3.2(b). The sign of this factor and the stable solutions can be found numerically. These results were compared with those from numerical simulations and this will be presented shortly. Now, however, we want to turn our attention to the problem of finding the phase distribution of the steady state field.

3.4 Phase distribution

Knowing the field density matrix at given time the phase distribution of the field can be calculated. The probability that the phase is within the interval $\lambda, \lambda + d\lambda$ is $\langle\lambda|\hat{\rho}|\lambda\rangle d\lambda$, where $|\lambda\rangle$ is the quantum-mechanical phase state [18]

$$|\lambda\rangle \equiv \frac{1}{\sqrt{2\pi}} \sum_{n=0}^{\infty} \mathrm{e}^{\mathrm{i}n\lambda}|n\rangle. \tag{3.22}$$

Therefore, the phase distribution is defined by the diagonal density matrix elements $\langle\lambda|\hat{\rho}|\lambda\rangle$. The core of our approach to determining the phase distribution lies in using the special orthogonal atomic states

$$|\pm\rangle \equiv \frac{1}{\sqrt{2}}(\mathrm{e}^{-\mathrm{i}\varphi}|a\rangle \pm |b\rangle), \tag{3.23}$$

as the atomic basis. These states are actually the eigenstates of the semiclassical interaction Hamiltonian which is obtained by replacing the operators a ($a^\dagger$) in the interaction term of Eq. (2.1) by the c-number field amplitude v (v^*), $v = |v|\mathrm{e}^{-\mathrm{i}\varphi}$,

$$H_{\mathrm{int,sc}} = g(\sigma^- v^* + \sigma^+ v). \tag{3.24}$$

The dynamics of these states was intensively studied within the context of the Jaynes-Cummings model by Gea-Banacloche [17] who discovered the formula which describes their time evolution in the limit of large photon number $\bar{n}$. On a time scale which is much smaller than the revival time $t_r = 2\pi\sqrt{\bar{n}}/g$. if the micromaser field is prepared in the coherent state $|v\rangle$, where $v = \sqrt{\bar{n}}e^{-i\varphi}$. then $|\pm\rangle|v\rangle$ evolves as

$$|\pm\rangle|v\rangle \rightarrow e^{\mp i\frac{gt\sqrt{n}}{2}}|\pm\rangle|ve^{\mp i\frac{gt}{2\sqrt{n}}}\rangle. \tag{3.25}$$

The error in Eq. (3.25) is of order $1/\sqrt{\bar{n}}$. This result provides a convenient way of treating the systems with large photon number, because the total state vector remains a product of atomic and the field parts.

An arbitrary atomic state can be expressed as

$$|\Psi\rangle = e^{-iw}\sin\kappa|a\rangle + \cos\kappa|b\rangle, \tag{3.26}$$

which in the basis of $|\pm\rangle$ states becomes

$$|\Psi\rangle = \langle +;\varphi|\Psi\rangle|+;\varphi\rangle + \langle -;\varphi|\Psi\rangle|-;\varphi\rangle, \tag{3.27}$$

where the explicit phase dependence of states $|\pm\rangle$ has been included. The coefficients of this expansion can be found easily

$$|\langle +;\varphi|\Psi\rangle|^2 = \frac{1}{2}(1+\cos(w-\varphi)\sin(2\kappa))$$

$$|\langle -;\varphi|\Psi\rangle|^2 = \frac{1}{2}(1-\cos(w-\varphi)\sin(2\kappa)). \tag{3.28}$$

For any initial atomic state, $|\Psi\rangle$, Eq. (3.25) can be employed for finding the total state of the system at later time. We are concerned with the steady state micromaser field, and its phase in particular, therefore we shall need the evolution of the field density matrix $\hat{\rho}$. The initial density matrix of the system $\hat{\rho}_{\rm system} = |v\rangle|\Psi\rangle\langle\Psi|\langle v|$ evolves in time according Eq. (3.25) too, of course, and it provides the field density operator after we take trace with respect to the atomic degrees of freedom. We obtain

$$|v\rangle\langle v| \to |\langle +;\varphi|\Psi\rangle|^2|e^{-i\delta\varphi}v\rangle\langle e^{-i\delta\varphi}v| + |\langle -;\varphi|\Psi\rangle|^2|e^{i\delta\varphi}v\rangle\langle e^{i\delta\varphi}v|. \tag{3.29}$$

where $\delta\varphi = g\tau/2\sqrt{\bar{n}}$. In order to find the steady state phase distribution of the field, the P-representation of the density matrix may be used. The P-representation is a diagonal representation of $\hat{\rho}$ in terms of coherent states,

$|\xi\rangle$, as $\hat{\rho} = \int d^2\xi P(\xi)|\xi\rangle\langle\xi|$. Using this, we can convert Eq. (3.29) into an equation for $P(v)$

$$P(v) \to |\langle\Psi|+;\varphi-\delta\varphi\rangle|^2 P(v\mathrm{e}^{\mathrm{i}\delta\varphi}) + |\langle\Psi|-;\varphi+\delta\varphi\rangle|^2 P(v\mathrm{e}^{-\mathrm{i}\delta\varphi}). \qquad (3.30)$$

It is apparent that the Eq. (3.30) describes merely changes of the field phase. the field amplitude is unaffected, so that we drop the explicit $|v|$ dependence in $P(|v|\mathrm{e}^{-\mathrm{i}\varphi})$. With the help of Eq. (3.28) we find

$$\begin{aligned} P(\varphi) \quad \to \quad & \frac{1}{2}(1+\cos(w-\varphi+\delta\varphi)\sin 2\kappa)P(\varphi-\delta\varphi) \\ & +\frac{1}{2}(1-\cos(w-\varphi-\delta\varphi)\sin 2\kappa)P(\varphi+\delta\varphi). \end{aligned} \qquad (3.31)$$

The right hand side of Eq. (3.31) must be equal to $P(\varphi)$ for the steady state field. For a large $\bar{n}$ we have $\delta\varphi \ll 1$, therefore we expand the right hand side of Eq. (3.31) up to the second order of $\delta\varphi$ and then the steady state condition give us the second order differential equation for $P(\varphi)$

$$0 = -\frac{d}{d\varphi}[P(\varphi)\cos(w-\varphi)\sin 2\kappa] + \frac{1}{2}\frac{d^2}{d\varphi^2}P(\varphi)\delta\varphi. \qquad (3.32)$$

This can be integrated giving the periodic solutions

$$P(\varphi) = C' e^{-\frac{2\sin 2\kappa}{\delta\varphi}\sin(w-\varphi)}, \tag{3.33}$$

where C' is the constant of integration. Note, that even though the formal solution to Eq. (3.32) has two constants, one of them is eliminated by the requirement of periodicity. The solutions given by Eq. (3.33) allow us to draw several conclusions. First, without even knowing C', one can immediately find the position of the maximum of the phase distribution

$$\varphi_{\max} = w - \frac{3\pi}{2}. \tag{3.34}$$

Second, the phase probability distribution $R(\lambda) \equiv \langle\lambda|\hat{\rho}|\lambda\rangle$ can be calculated from

$$R(\lambda) = \int d^2\xi P(\xi)|\langle\xi|\lambda\rangle|^2. \tag{3.35}$$

The coherent state in the number-state representation is defined as [19]

$$|\xi\rangle \equiv e^{-\frac{|\xi|^2}{2}} \sum_{n=0}^{\infty} \frac{\xi^n}{\sqrt{n!}}|n\rangle, \tag{3.36}$$

and then from Eq. (3.35) we obtain final expression for $R(\lambda)$ ($r = \sqrt{\bar{n}}$)

$$R(\lambda) = \frac{C}{2\pi} e^{-r^2} \sum_{n,m=0}^{\infty} \frac{r^{m+n}}{\sqrt{m!n!}} \int_0^{2\pi} d\varphi \cos((\varphi + \lambda)(n-m)) e^{-\frac{2\sin 2\kappa}{\delta\varphi}\sin(w-\varphi)}. \tag{3.37}$$

The constant C is determined from the normalization condition

$$\int_0^{2\pi} R(\lambda) d\lambda = 1. \tag{3.38}$$

The integral with respect to λ is

$$\int_0^{2\pi} d\lambda \cos((\varphi + \lambda)(n-m)) = 2\pi\delta_{nm}, \tag{3.39}$$

where δ_{nm} is the Kronecker symbol, so that we have finally

$$C = \left[\int_0^{2\pi} d\varphi e^{-\frac{2\sin 2\kappa}{\delta\varphi}\sin(w-\varphi)}\right]^{-1}. \tag{3.40}$$

The results from the numerical simulations, that are presented in the following section, show that Eq. (3.37) is very precise when $\bar{n}$ is large.

3.5 Numerical results

In the most of the following numerical experiments the atom-field interaction constant g was $4.4 \times 10^4 Hz$ and the relative phase of the coherent atomic state u (as defined by Eq. (3.26)) was set to 0. The pumping statistics was chosen to be regular, because the Poissonian case is computationally very demanding. We shall comment on the effect this has on our results shortly.

We studied how the steady-state field varies with respect to the micromaser parameters $\mathcal{N}_{\rm ex}$, $\theta_{\rm int}$ and $|\alpha|$. Table 3.1 will help with the following discussion. In Figure 3.3 we plot the mean photon number $\bar{n}$ in the steady-state as a function of $\theta_{\rm int}$ when $\mathcal{N}_{\rm ex} = 30$ and $|\alpha| = 0.9$. The $\theta_{\rm int}$ interval was evenly sampled by 201 points points between 0 and 40. For each value of $\theta_{\rm int}$ we found $\bar{n}$ performing following procedure. The initial state of the cavity field was taken to be the vacuum. The field then interacted with an atom according to Eq. (2.21), and then decayed according to Eq. (2.26). The measurement of the field's mean photon number $\bar{n}$ was performed just before next atom entered the cavity. This sequence, corresponding to Eq. (2.28), was repeated until the steady state value of $\bar{n}$ was found. The field was considered steady when its $\bar{n}$ changed by less than $10^{-3}\%$ during single sequence. The reason behind this is that we had to set an upper bound for the num-

ber of interactions in order to get the results in reasonable time; for smaller N_{ex} (30 to 100) it was set to $30 \times N_{ex}$ and for larger N_{ex} it was $15 \times N_{ex}$. If $\bar{n}$ changes at a rate of $10^{-3}\%$ per sequence, then the field would need to interact with 10^5 atoms to increase its value by one. This means that such small differences would not show up on the graphs, even if we considered the maximum number of interactions to be 7500 ($N_{ex} = 500$).

The points from the quantum-mechanical simulations are in Figure 3.3 are joined by a continuous line. The crosses on the same figure show semiclassical stable solutions as given by Eq. (3.19). We find a very good correspondence between the two when θ_{int} is between 0 and 5. The two curves are almost identical in the vicinity of the first micromaser threshold where $\bar{n}$ has its maximum. The quantum-mechanical line shows the second threshold around $\theta_{int} = 10$, and beyond this point it doesn't match the semiclassical pattern. The relationship between $\bar{n}$ and θ_{int} was also studied for $N_{ex} = 100, 300$ and 500; the results are shown in Figures 3.4,3.6,3.10. As N_{ex} increases the second threshold moves to larger values of θ_{int}, for example, when $N_{ex} = 500$ it occurs around $\theta_{int} = 37$, while the quantum-mechanical and the semiclassical solutions coincide for larger intervals of θ_{int}. Therefore, we may conclude that our semiclassical theory gives correct predictions for $\bar{n}(\theta_{int})$ provided that N_{ex}

is large.

We were also concerned with the questions of how $\bar{n}(\theta_{\rm int})$ and the relationship between the quantum-mechanical and the semiclassical solutions depend on $|\alpha|$. To answer this question four simulations were done setting $|\alpha|$ to 0.85, 0.9, 0.95 and 1.0 with $N_{\rm ex} = 300$. The results are plotted in Figures 3.5,3.6,3.7,3.8. As one can see, the second threshold occurs at smaller $\theta_{\rm int}$ as $|\alpha|$ increases. Up to that point the quantum-mechanical and the semiclassical curves are almost identical.

A careful reader has probably noticed that we were using different pumping statistics for the semiclassical theory and for the numerical simulations. He may ask whether our comparison is reasonable and how much the results of the semiclassical theory depend on the pumping statistics. In order to investigate this point we shall find the semiclassical stable solutions for the amplitude and the phase of the steady-state field for a micromaser with regular pumping. If it is assumed that the measurements are performed just before the pumping atoms enter the cavity, Figure 2.3 (a), then the steady-state condition gives

$$\langle a(t_{i+1})\rangle = \langle a(t_i)\rangle, \tag{3.41}$$

which can be expressed with help of Eq. (2.28) as

$$\mathrm{Tr}\{\mathrm{e}^{LT}M\hat{\rho}(t_i)a\} = \mathrm{Tr}\{\hat{\rho}(t_i)a\}. \tag{3.42}$$

Following the procedure from Sec. 3.2 and 3.3, we find that the phase θ of the steady-state field is

$$\theta = \phi + \pi, \tag{3.43}$$

and the amplitude of the field can be determined from

$$u - u' = \frac{1}{2u'}(|\alpha|^2 - |\beta^2|)s_{\bar{n}'}^2 + |\alpha\beta|\frac{s_{\bar{n}'}c_{\bar{n}'}}{u'}, \tag{3.44}$$

where

$$u' = \mathrm{e}^{-1/2N_{\mathrm{ex}}}u. \tag{3.45}$$

The same notation as in Eqs. (3.1), (3.13) was used. The stability analysis gives us time evolution of δn and $\delta\theta$ in terms of the maps

$$\delta u \to \frac{1}{u}\left[2u' - u + \{(|\alpha|^2 - |\beta|^2)s_{\bar{n}'}c_{\bar{n}'} + |\alpha\beta|(c_{\bar{n}'}^2 - s_{\bar{n}'}^2)\}\frac{\theta_{\mathrm{int}}}{\sqrt{N_{\mathrm{ex}}}}\right]\delta u. \tag{3.46}$$

$$\delta\theta \to \left[1 - |\alpha\beta|\frac{\theta_{\mathrm{int}}}{u\sqrt{N_{\mathrm{ex}}}}\right]\delta\theta. \tag{3.47}$$

We have plotted the stable points for the case with $|\alpha| = 1.0$ and $N_{\rm ex} = 300$ in Figure 3.8, and we see that they come very close to those calculated with Poissonian pumping. We further find that the points for the both kinds of pumping statistics stay close for large $N_{\rm ex}$, and they only start to differ as $\theta_{\rm int}$ increases. However, even for small $N_{\rm ex}$ (such as 30) they both provide almost the same values of $\bar{n}$ for $\theta_{\rm int}$ around the first threshold, which is also in very good correspondence with the quantum-mechanical simulations, Figure 3.8. Therefore we conclude that the pumping statistics does not play a role in the semiclassical treatment of the micromaser if the objective is to determine the mean photon number of the steady-state field for values of $\theta_{\rm int}$ of order 1. We prefer to work with Poissonian pumping because it corresponds better to the actual physical experiments.

The next question we would like to ask is: will the pumping statistics make a bigger difference in the quantum-mechanical treatment of the micromaser? The probabilities p_n of the steady-state field having n photons for the micromaser with Poissonian pumping can be found analytically [20]

$$p_n = p_0 \prod_{m=1}^{n} \frac{\rho_{aa} s_m^2}{\rho_{bb} s_m^2 + m/N_{\rm ex}}, \tag{3.48}$$

where p_0 is determined from the normalization condition

$$\sum_{n=0}^{\infty} p_n = 1. \tag{3.49}$$

This formula is valid for the situation when the pumping atoms are in the mixed state: $\rho_{aa}|a\rangle\langle a| + \rho_{bb}|b\rangle\langle b|$. The formula was used for calculating $\bar{n}(\theta_{\rm int})$. Figure 3.9. We set $\rho_{aa} = 1$ in order to compare the resulting points to our simulations (note that we use pure atomic states there). The figure shows the second, the third and higher thresholds where, according to the analogy with statistical physics, the micromaser field undergoes the first-order phase transition. Comparing with Figures 3.8 and 3.9, we see that the curves corresponding to the quantum mechanical results for regular and Poissonian pumping are very different, they coincide around the first threshold only. Therefore, the pumping statistics do have a remarkable effect in the quantum-mechanical theory.

So far, it was found that the semiclassical predictions agree very well with the quantum-mechanical simulations in the region around the first threshold where the mean photon number reaches its maximum values. It was supposed in the analytical treatment that the steady-state field is coherent, for which

Figure	$\|\alpha\|$	N_{ex}	Pumping	
			QM points	SC stable points
3.3	0.9	30	regular	Poissonian
3.4	0.9	100	regular	Poissonian
3.5	0.85	300	regular	Poissonian
3.6	0.9	300	regular	Poissonian
3.7	0.95	300	regular	Poissonian
3.8	1.0	300	regular	Poissonian, regular
3.9	1.0	300	Poissonian	Poissonian
3.10	0.9	500	regular	Poissonian

Table 3.1: List of figures with results from numerical simulations at glance, relevant to the discussion about relationship between average photon number $\bar{n}$ and pumping parameter $\theta_{\rm int}$. In the two last columns QM, SC means quantum-mechanical and semiclassical respectively.

$\bar{n} = |\eta|^2$ and the root-mean-squared deviation of the photon distribution $\sigma = |\eta|$, where η is its amplitude. We can examine this assumption by calculating the values of $\sigma/\sqrt{\bar{n}}$ and $|\langle a\rangle|^2/\bar{n}$ as a functions of $\theta_{\rm int}$, and these are plotted in Figure 3.11 for the steady-state field of the micromaser with $N_{ex} = 300$ and $|\alpha| = 0.9$. Both curves are smooth on the region between 0 and 15 approximately, which corresponds to the area around the first threshold. The values of $|\langle a\rangle|^2/\bar{n}$ are close to 1, also $\sigma/\sqrt{\bar{n}}$ is almost constant on the largest portion of the region though smaller than 1. Therefore, our assumption about the strong steady-state micromaser field is justified, indeed.

At last, we want to check the validity of Eq. (3.37). We present results from two simulations; in both cases $|\alpha| = 0.9$ and $w = 0$. Figure 3.12 shows

the phase distribution of the steady-state field for $N_{ex} = 30$; it was chosen so that $\theta_{int} = 1.12$ since it provides large mean photon number, $\bar{n} = 23.6$, which gives $\delta\varphi = 0.0253$. The values of $\delta\varphi$ and $\bar{n}$ were used when calculating the distribution from Eq. (3.37), where we set the upper limit for the indices m, n to 50. The resulting curve matches very well the phase distribution from the numerical simulations. We find some differences only at the tip of the peak where the analytical one is slightly taller, approximately by 5%. The second comparison, Figure 3.13, is for the situation when $N_{ex} = 100$, $\theta_{int} = 1.2$ and $\bar{n} = 80.3$ for which $\delta\varphi = 6.70 \times 10^{-3}$. Also here the analytical distribution agrees very well with the numerical simulations. The peak is narrower and we see some differences only at its tip. Experimenting more with the parameters it was found that Eq. (3.37) provides excellent results for large $\bar{n}$; values of $\bar{n}$ as small as 15 provide good agreement. For θ_{int} where $\bar{n}$ was smaller, the peak became less pronounced and the values started to depart from those obtained from the simulations.

3.6 Conclusions

Our semiclassical theory provides results that are in very good agreement with the quantum-mechanical numerical simulations when the cavity field has a large mean photon number. The stable solutions for the mean photon number as a function of the interaction parameter θ_{int} coincide with the simulations on the interval whose size increases as N_{ex} increases while keeping $|\alpha|$ constant. On the other hand, while keeping N_{ex} constant, the interval of validity becomes larger as $|\alpha|$ decreases. The average photon number reaches its maximum, which is equal to $|\alpha|^2 N_{\text{ex}}$, at the first threshold. Then as θ_{int} increases the semiclassical result continues to follow the quantum-mechanical dependence approximately until the latter reaches a second threshold. Also, it was found that the pumping statistics does not play a significant role in the semiclassical treatment if the objective is to determine only the mean photon number. Of course, the same can not be said about the quantum case.

The semiclassical approximation for the phase distribution is in very good agreement with the quantum mechanical one. It was shown that it is sufficient to have as few as 15 photons in the steady field to obtain a precise result. The expression for the phase distribution depends on the mean photon

number as a parameter. That can be determined using the stable semiclassical solution from Section 3.3. Therefore, the presented theory is complete allowing one to obtain results using only the parameters, such as $N_{\rm ex}$ and $\theta_{\rm int}$, which specify the micromaser.

The present treatment, however, cannot be used to determine the photon number distribution, and this remains a challenge and motivation for further work.

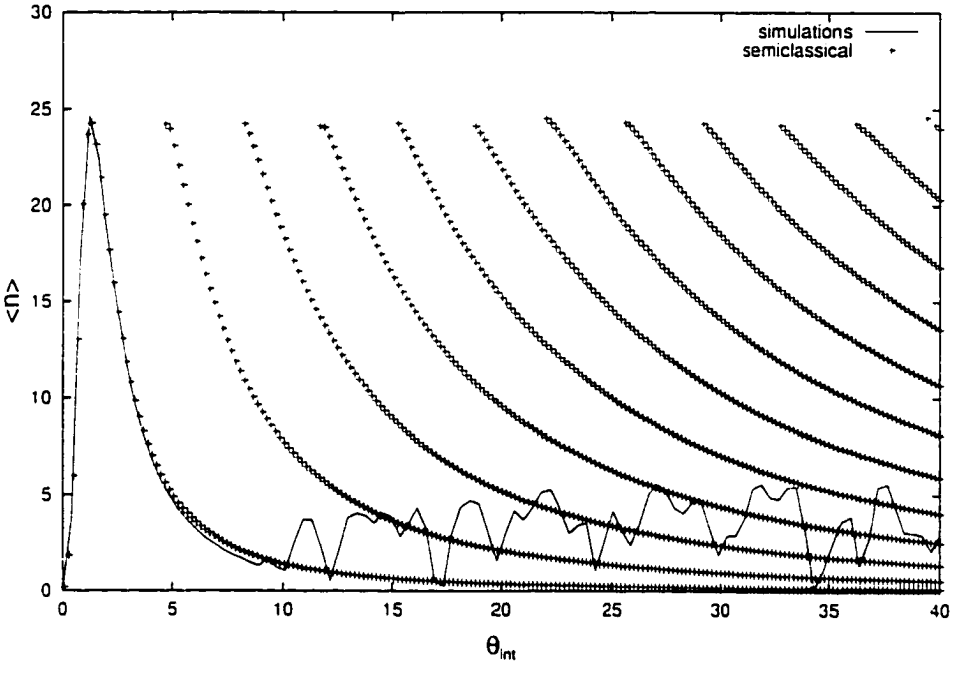

Figure 3.3: Mean photon number $\bar{n}$ of the steady state field versus the pumping parameter $\theta_{\rm int}$, $|\alpha| = 0.9$ and $N_{\rm ex} = 30$. The points from the quantum mechanical simulations with regular pumping are joined by the continuous line, while the crosses show semiclassical stable solutions where Poissonian pumping was assumed.

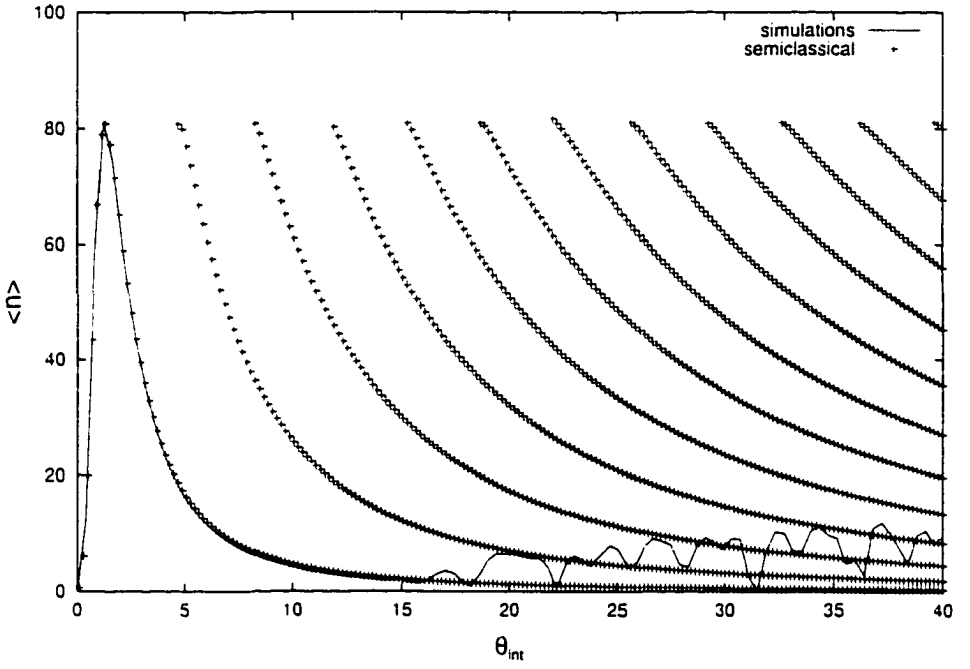

Figure 3.4: Mean photon number $\bar{n}$ of the steady state field versus the pumping parameter $\theta_{\rm int}$, $|\alpha| = 0.9$ and $N_{\rm ex} = 100$. The points from the quantum mechanical simulations with regular pumping are joined by the continuous line, while the crosses show semiclassical stable solutions where Poissonian pumping was assumed.

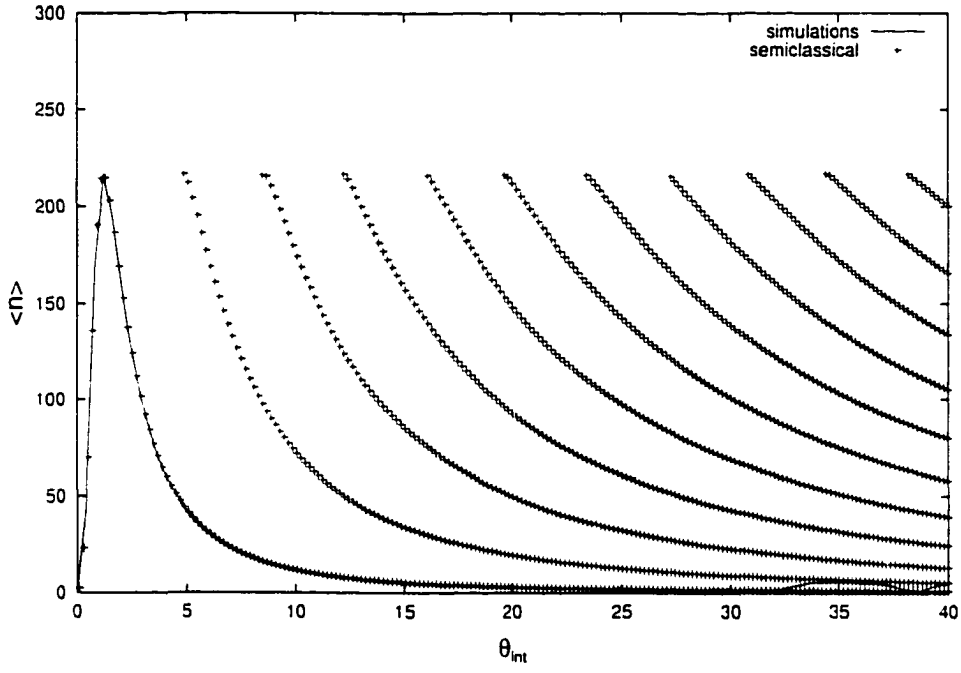

Figure 3.5: Mean photon number $\bar{n}$ of the steady state field versus the pumping parameter θ_{int}, $|\alpha| = 0.85$ and $N_{\text{ex}} = 300$. The points from the quantum mechanical simulations with regular pumping are joined by the continuous line, while the crosses show semiclassical stable solutions where Poissonian pumping was assumed.

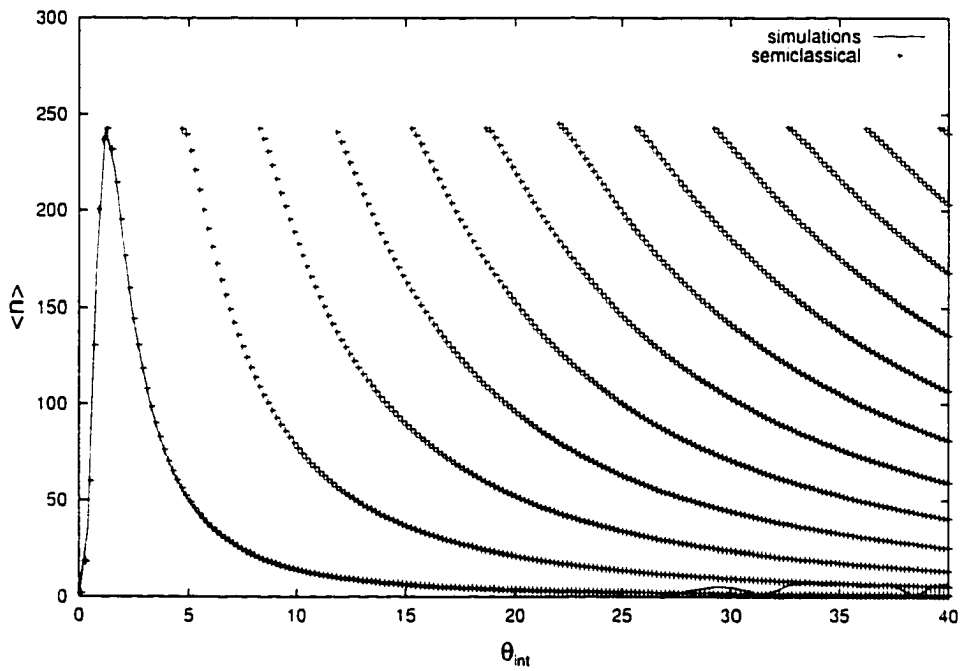

Figure 3.6: Mean photon number $\bar{n}$ of the steady state field versus the pumping parameter $\theta_{\rm int}$. $|\alpha| = 0.9$ and $N_{\rm ex} = 300$. The points from the quantum mechanical simulations with regular pumping are joined by the continuous line, while the crosses show semiclassical stable solutions where Poissonian pumping was assumed.

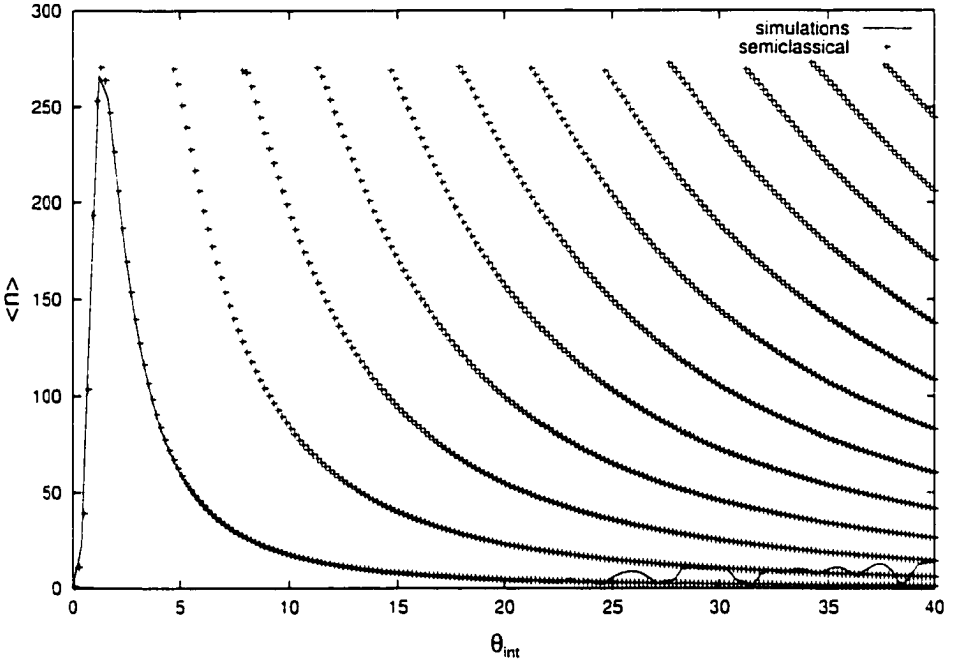

Figure 3.7: Mean photon number $\bar{n}$ of the steady state field versus the pumping parameter $\theta_{\rm int}$, $|\alpha| = 0.95$ and $N_{\rm ex} = 300$. The points from the quantum mechanical simulations with regular pumping are joined by the continuous line, while the crosses show semiclassical stable solutions where Poissonian pumping was assumed.

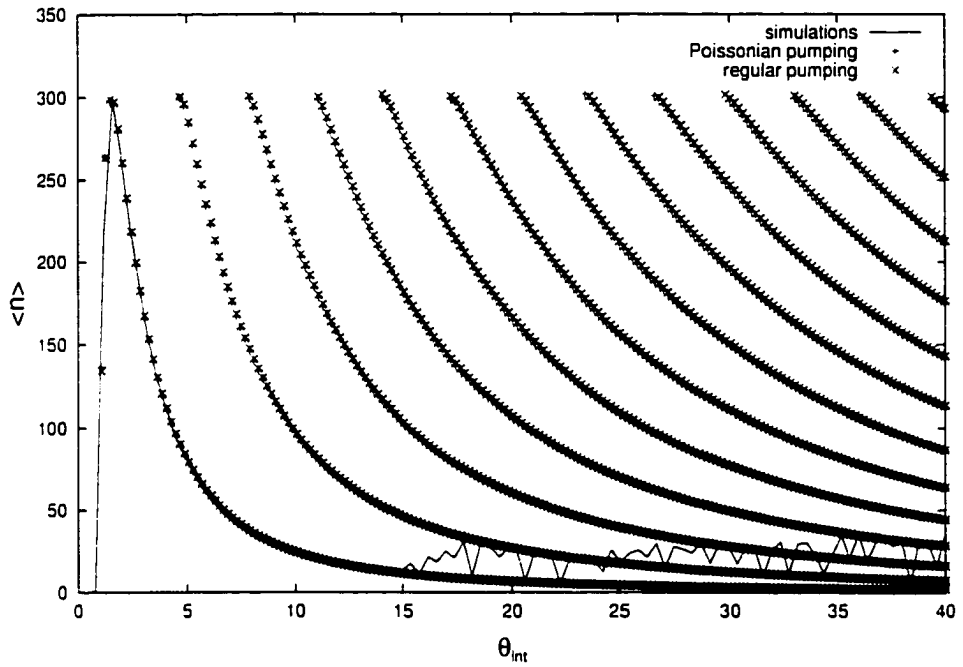

Figure 3.8: $\bar{n}$ Vs. $\theta_{\rm int}$ for the case with $|\alpha| = 1.0$ and $N_{\rm ex} = 300$. The continuous line joins the steady state points gained from the quantum mechanical simulation with regular pumping. The two types of crosses now show *semiclassical* stable solutions for both Poissonian and regular pumping. For larger values of $N_{\rm ex}$ the two almost coincide.

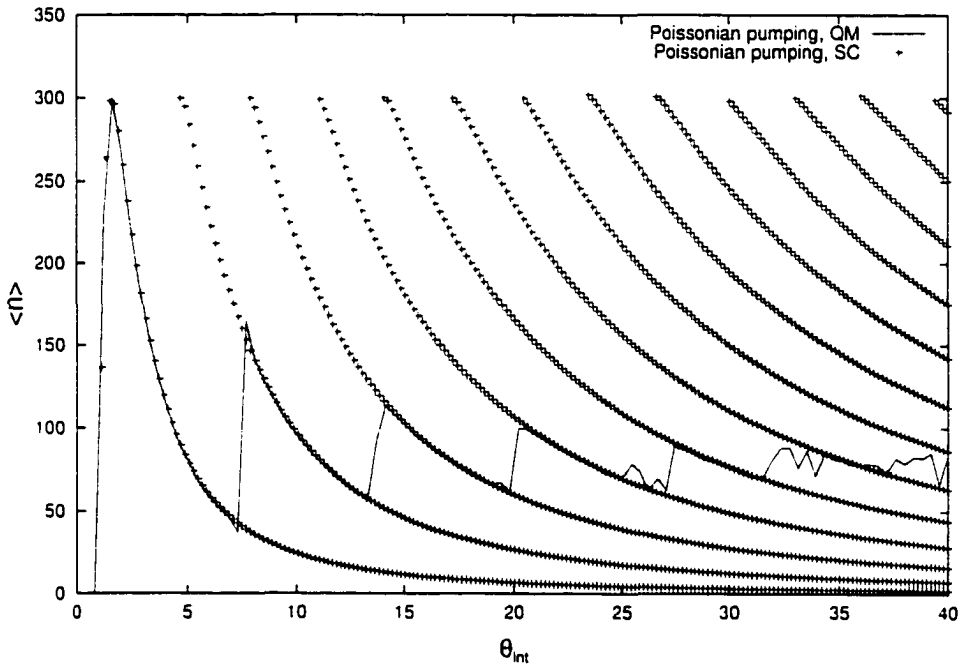

Figure 3.9: $\bar{n}$ Vs. $\theta_{\rm int}$ for the case with $|\alpha| = 1.0$ and $N_{\rm ex} = 300$. The continuous line now represents analytical *quantum mechanical* solutions for Poissonian pumping. The crosses stand for the semiclassical stable points. The quantum mechanical curve is quite different from the previous cases with regular pumping.

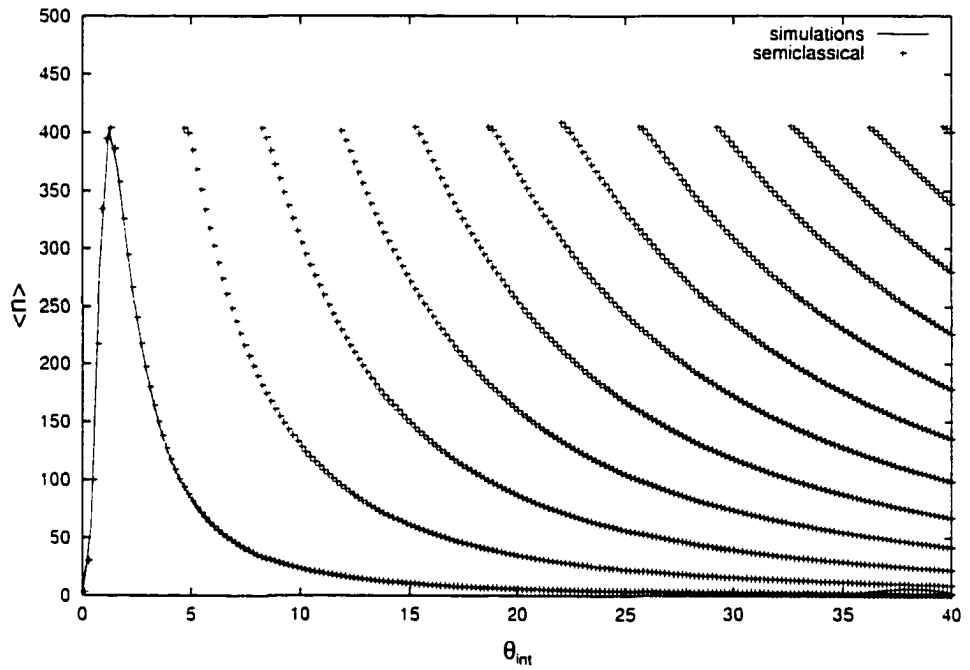

Figure 3.10: Mean photon number $\bar{n}$ of the steady state field versus the pumping parameter θ_{int}, $|\alpha| = 0.9$ and $N_{\text{ex}} = 500$. The points from the quantum mechanical simulations with regular pumping are joined by the continuous line, while the crosses show semiclassical stable solutions where Poissonian pumping was assumed.

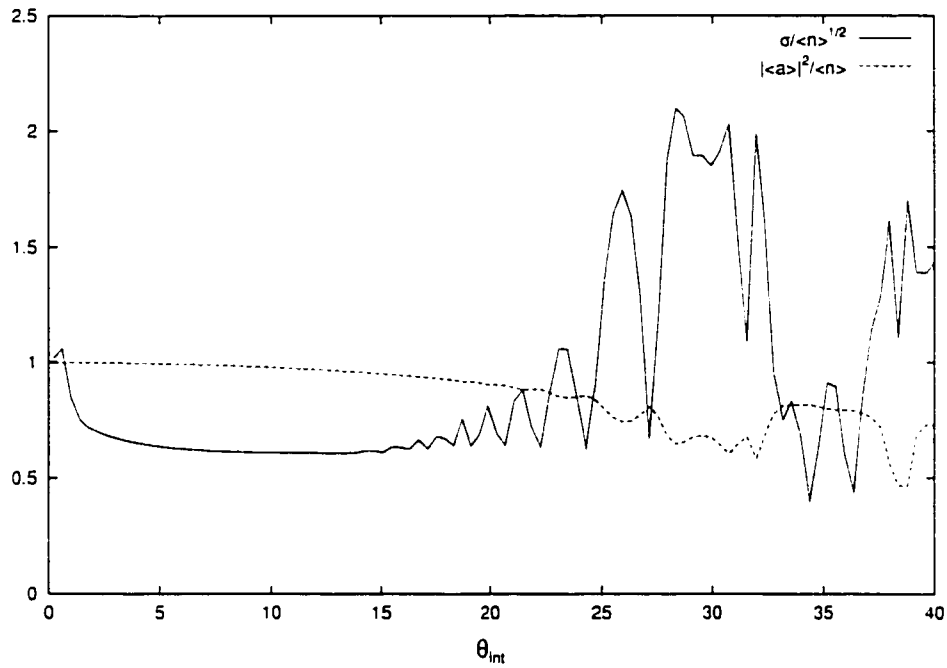

Figure 3.11: The normalized root-mean-squared deviation $\sigma/\sqrt{\bar{n}}$ of the photon number of the steady state field versus the pumping parameter θ_{int} is plotted by the continuous line, while the dashed line shows the ratio $|\langle a\rangle|^2/\bar{n}$ vs. θ_{int}. Within the interval $(0, 15)$ approx. the value is close to 1, which shows that the field is almost coherent. $N_{\text{ex}} = 300$ and $|\alpha| = 0.9$.

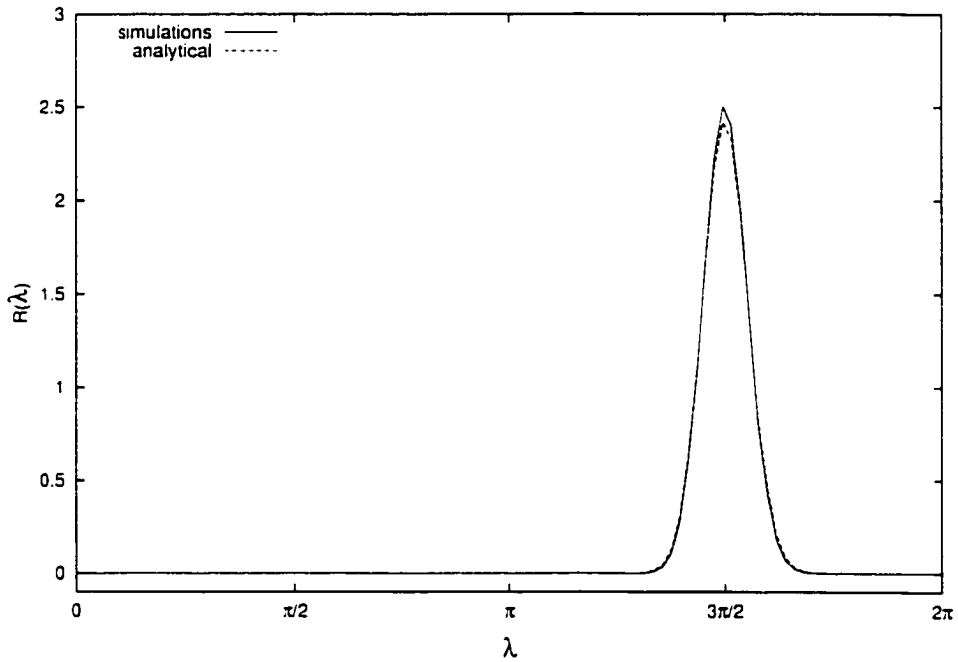

Figure 3.12: Phase distribution of the steady-state field. Data from the numerical simulations is shown by the continuous line, the dashed line shows results from Eq. (3.37). This is the case with $N_{\rm ex} = 30$, $|\alpha| = 0.9$ and $\theta_{\rm int} = 1.12$.

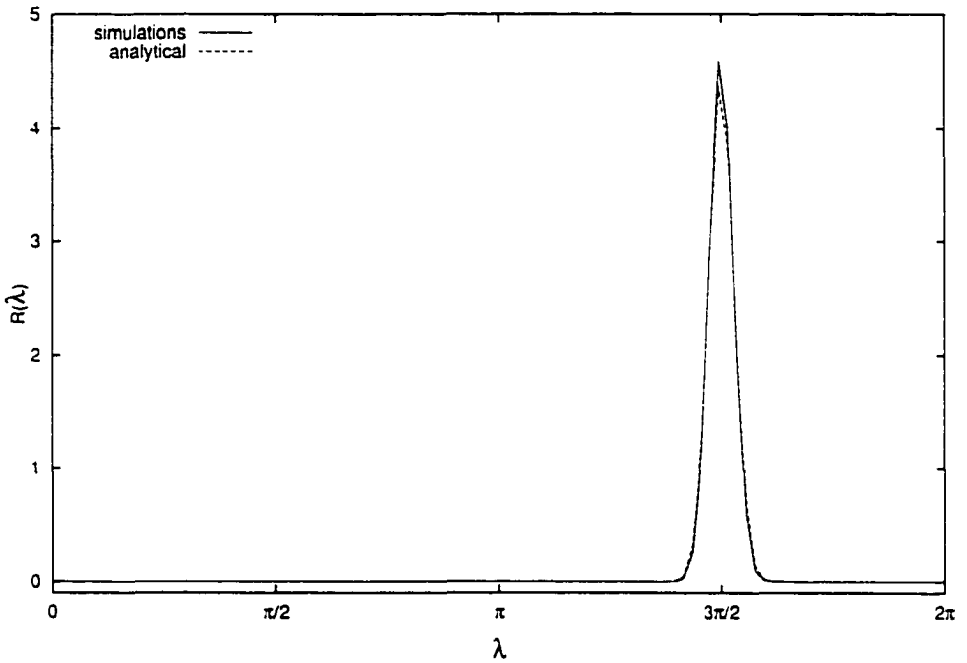

Figure 3.13: Phase distribution of the steady-state field. Data from the numerical simulations is shown by the continuous line, the dashed line shows results from Eq. (3.37). This is the case with $N_{ex} = 100$, $|\alpha| = 0.9$ and $\theta_{int} = 1.2$.

Chapter 4

Field oscillations

4.1 Introduction

Extensive theoretical work on the micromaser, see Chapter 1, has shown the existence of numerous interesting features. Among them are trapping states, which separate the dynamics into noninteracting blocks of photon numbers [2], and the dependence of steady state of the field on the injection statistics of the atoms [21]. The latter occured as part of more general analysis of pump noise in lasers and masers, and how to minimize it [22, 23]. Despite all of this, however, there are still some surprises. One, found only recently, involves the behavior of the electric field inside the cavity. It has

been found by Briegel, Englert, and Scully [24], and independently by Herzog and Bergou [25], that the passage of a single atom can cause the sign of the electric field to flip. They demonstrated this by calculating the two-time field-field correlation function and showing that it can change sign. For a micromaser with regular pumping (equal time intervals between atoms) this effect causes a splitting of the spectrum into several equidistant peaks. In this work the atoms were injected into the cavity in their upper states. Another kind of field oscillation was found by Slosser and Meystre when the atoms are injected in a coherent superposition of their upper and lower states [10]. Considering a lossless micromaser, they found steady states for the field which they called tangent and cotangent states (the names refer to the form of coefficients when the states are expanded in the number-state basis), which are confined between trapping states [2]. They then went on to examine the dynamics of the system when the photon numbers were limited by two trapping states. They found, numerically, that if other trapping states intervened between the original two, there were states which one might call steady states of period 2; these states are mapped back onto themselves not by the interaction with one atom, as a normal steady state would be, but by the interaction with two atoms. The electric field of such a state oscillates

between two values; it changes its value after the passage of one atom and returns to its original value after the passage of a second.

Here we would like to give a simple explanation for the oscillations seen by Slosser and Meystre. This explanation hinges on a slight difference in the behavior of tangent and cotangent states after the passage of an atom. In addition we wish to see how the oscillatory behavior is affected by the presence of losses. In Section 4.2 we examine the lossless case while the effects ot the losses are considered in Section 4.3.

4.2 Lossless micromaser

We shall consider a micromaser in which the pumping atoms are injected at regular time intervals, with the time between atoms being T. Strictly speaking, this assumption is not necessary for our analysis in the lossless case to be valid. However, when we do consider losses it will be necessary to make a particular choice for the injection statistics, and this is the choice we shall make. Each atom interacts with the field for a time, τ, which is much smaller than T. Between atoms the field evolves freely, while during the time an atom is in the cavity the interaction of the field and the atom is governed

by the Jaynes-Cummings Hamiltonian as given in Chapter 2, see Eq. (2.1). The total state vector of the system evolves according Eq. (2.18)

$$|f\rangle \otimes (\alpha|a\rangle + \beta|b\rangle) \rightarrow \sum_{n=0}^{\infty} d_n(\alpha c_{n+1}|n\rangle - i\beta s_n|n-1\rangle) \otimes |a\rangle + \sum_{n=0}^{\infty} d_n(\beta c_n|n\rangle - i\alpha s_{n+1}|n+1\rangle) \otimes |b\rangle.$$

if the initial state of the atom and the field is described by Eq. (2.16) and Eq. (2.17) respectively.

Slosser and Meystre found the tangent and cotangent states by demanding that the state on the right-hand side of the Eq. (2.18) be a product of the original field state and an atomic state, i. e. that

$$|f\rangle \otimes (\alpha|a\rangle + \beta|b\rangle) \rightarrow |f\rangle \otimes (\alpha'|a\rangle + \beta'|b\rangle). \tag{4.1}$$

This condition guarantees that the field state is unchanged by the passage of an atom. They found that this condition is satisfied if either $\alpha' = -\alpha$, $\beta' = \beta$, and

$$d_n = -i\frac{\alpha}{\beta}\cot(g\tau\sqrt{n}/2)d_{n-1}, \tag{4.2}$$

(cotangent state) or if $\alpha' = \alpha$, $\beta' = -\beta$, and

$$d_n = i\frac{\alpha}{\beta}\tan(g\tau\sqrt{n}/2)d_{n-1}, \tag{4.3}$$

(tangent state). The tangent and cotangent states are normalizeable only if the sums over number states are restricted to a finite range. Expressing both states as

$$|f\rangle = \sum_{n=N_d}^{N_u} d_n|n\rangle, \tag{4.4}$$

and imposing the conditions $d_{N_d-1} = 0$ and $d_{N_u+1} = 0$, we find that

$$g\tau\sqrt{N_u+1} = p\pi \qquad\qquad g\tau\sqrt{N_d} = q\pi, \tag{4.5}$$

where p and q are integers. For tangent states p is even and q is odd, while for cotangent states p is odd and q is even.

The results of the preceding paragraph imply that for a tangent state, $|f_t\rangle$,

$$|f_t\rangle \otimes (\alpha|a\rangle + \beta|b\rangle) \rightarrow |f_t\rangle \otimes (\alpha|a\rangle - \beta|b\rangle), \tag{4.6}$$

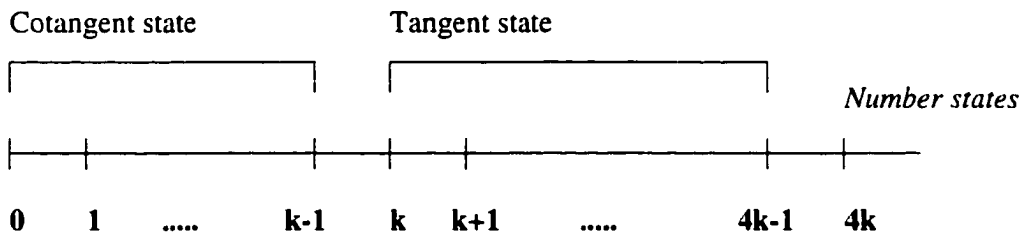

Figure 4.1: Cotangent and tangent states. The state $|k\rangle$ is π trapping state. $g\tau\sqrt{k} = \pi$.

and for a cotangent state, $|f_c\rangle$,

$$|f_c\rangle \otimes (\alpha|a\rangle + \beta|b\rangle) \rightarrow -|f_c\rangle \otimes (\alpha|a\rangle - \beta|b\rangle). \tag{4.7}$$

If we have a state which is a superposition of a tangent and a cotangent state, $\xi_t|f_t\rangle + \xi_c|f_c\rangle$, see Figure 4.1, then after one atom passes through the cavity it becomes $\xi_t|f_t\rangle - \xi_c|f_c\rangle$ (where the states are defined up to a common sign), and after a second atom it returns to the original state. This state is then periodic with period 2 (where time is measured in units of T).

How can we see this oscillation of the state? Because of the conditions on N_d and N_u, tangent and cotangent states must exist in nonoverlapping blocks of number states. This means that the oscillations will not show up in observables which commute with the number operator. On the other hand, if the blocks are adjacent, then the electric field operator, which is proportional

to $(a^\dagger - a)$, can connect the two blocks, and the effect of the relative sign flip between them will manifest itself as an oscillation in the expectation value of the field. In order to see this explicitly let us look at the situation considered by Slosser and Meystre when $g\tau = \pi$, and there is a cotangent state at $n = 0$ (for certain values of the interaction time the vacuum satisfies the conditions necessary to be a cotangent state), a tangent state between 1 and 3, and a cotangent state between 4 and 8. The expectation value of the electric field in this state is

$$\langle E \rangle = i\sqrt{\frac{\omega}{2V}} \sum_{n=1}^{8} \sqrt{n}(\rho_{n-1,n} - \rho_{n,n-1}), \tag{4.8}$$

where V is the quantization volume, and ρ is the field density matrix. After passage of an atom a relative sign is introduced between the tangent state and the two cotangent states. This means that the density matrix elements between different blocks, ρ_{01}, ρ_{34}, and their complex conjugates, change sign while the others do not. This causes $\langle E \rangle$ to change. The passage of a second atom causes these density matrix elements to flip sign again, which restores $\langle E \rangle$ to its original value.

The periodicity of the state, then, does have observable effects. Besides the field one could also look at an observables such as $Y_1 = [a^2 + (a^\dagger)^2]/2$, $Y_2 = i[(a^\dagger)^2 - a^2]/2$ which appear in the study of some forms of higher- order

squeezing, and which also connect blocks. Because these connect the number states $|n\rangle$ and $|n+2\rangle$, rather than $|n\rangle$ and $|n+1\rangle$ as does the electric field operator, it will lead to a larger number of density matrix elements which flip sign and can thereby produce a larger effect.

4.3 Micromaser with losses

We now include losses in our system in order to see whether the steady-state oscillations which we discussed in the previous section will survive under under these more realistic conditions. Because the atom-field interaction time τ is much shorter than the time the cavity is empty, T, we shall ignore the effect of field losses during the times atoms are in the cavity. The decay of the micromaser field for the cavity at zero temperature is described by the master equation

$$\frac{\mathrm{d}\hat{\rho}}{\mathrm{d}t} = -\frac{1}{2}\gamma\left(a^{\dagger}a\hat{\rho} + \hat{\rho}a^{\dagger}a - 2a\hat{\rho}a^{\dagger}\right)$$

which was derived together with its solution in the number-state representation in Chapter 2.

We shall numerically simulate the system by using the Jaynes-Cummings dynamics to describe the atom-field interaction and the loss master equation

to describe the field during the periods during which the cavity is empty. The values of the micromaser parameters which we used in our numerical simulations were chosen to be as close as possible to those which occur in actual experiments [6]. The atom-field coupling constant g was set to $4.4 \times 10^4 Hz$, the time between two consecutive atoms was set to $T = 6.666 \times 10^{-3} s$, the cavity loss coefficient γ was set to $5 s^{-1}$, which provided cavity photon storage time $T_{cav} = 0.2 s$, and number of atoms passing through the cavity during a single decay time was taken to be $N_{ex} = 30$. The atom-field interaction time τ was varied in order to provide needed trapping condition, $g\tau = \pi$. The values of τ used in simulations came very close to the values in actual experiment [6].

Two-level atoms in the coherent superposition $\alpha|a\rangle + \beta|b\rangle$ are injected regularly into the micromaser cavity. The parameters α and β were chosen real with $\alpha = 0.9$. The cavity field was prepared initially in a state with a cotangent state at $n = 0$, a tangent state between 1 and 3, and a cotangent state between 4 and 8, using the same values of α, β as the pumping atoms. The starting values for the recurrence formulas (4.2,4.3) were optimized in order to provide large magnitudes of the observables of interest. Then the first atom was injected at $t = 0$, followed by much longer time period T

during which the field decayed. Then the second atom was injected followed by the cavity decay period and so on. The expectation values of observables were calculated after a decay time interval just before the injection of the next atom.

The expectation values of the electric field, operator Y_1 and Y_2 for the case are plotted in Figure 4.2. The interaction time is $\tau = 7.14 \times 10^{-5} s$ giving $\frac{\tau}{T} \cong 10^{-2}$, which justifies the assumption that we can neglect losses during the atom-field interaction. The pumping parameter $\theta_{int} = g\tau\sqrt{N_{ex}} \cong 17.2$. The mean value of each operator exhibits period-two oscillations, but with decreasing magnitude, because of the presence of damping. These expectation values eventually reach steady state values which do not exhibit oscillations. In addition, we found that the field approaches its steady state extremely slowly. This is caused by the presence of the trapping states which separate the total Fock space for the Jaynes-Cummings evolution into independent blocks. The probability flow between the subspaces in which the cotangent and tangent states are located occurs only because of the loss process, and it is very small.

We now look at the density matrix itself. The photon number distribution of the field, given by the diagonal density matrix elements, after the passage

of different numbers of atoms is shown in Figure 4.3. Note that the presence of damping drives the field toward lower photon numbers. In Figure 4.4 are plotted absolute values of the cavity field density matrix elements. Initially, because the system starts in a pure state, the density matrix has off-diagonal peaks. Because of the loss process, the off-diagonal elements of the density matrix decay as it approaches its new steady state. This new steady state is very different from the initial cotangent-tangent state, and this explains the deterioration of the oscillations in the expectation values of the operators, because they depend on the presence of the tangent and cotangent states which exhibit a relative phase oscillation.

Our conclusions on the effects of damping are consistent with the results of Slosser, Meystre, and Wright [11]. They considered a micromaser with Poissonian pumping and found that tangent and cotangent states maintain their integrity only in the limit of very large N_{ex}, i. e. very weak damping. For the damping which occurs in experiments, the damping drastically alters the character of the steady-state field.

4.4 Conclusions

We have shown that the period-two oscillations which exist in a lossless micromaser pumped by atoms in a coherent superposition of states are due to a relative sign change undergone by tangent and cotangent states upon passage of an atom through the cavity. These oscillations can only occur in observables, such as the electric field, which do not commute with the photon number operator. The addition of damping changes the oscillations from a steady-state to a transient phenomenon, but one with a rather long lifetime.

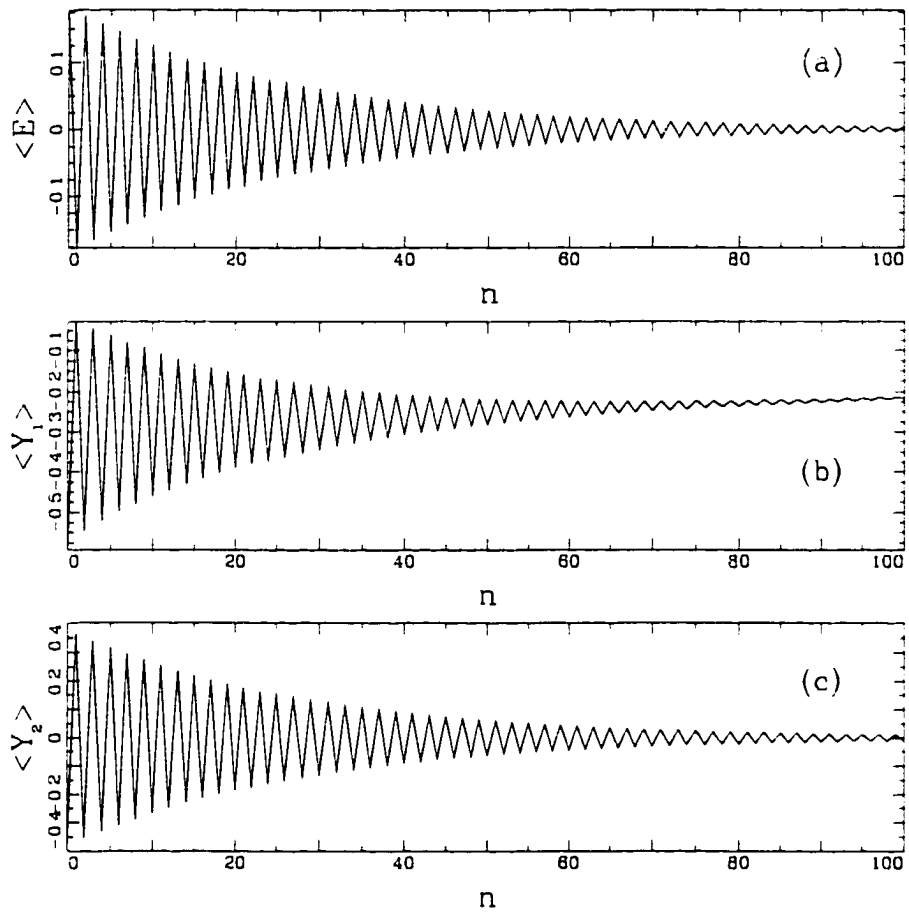

Figure 4.2: (a): Evolution of the expectation value of electric field $\langle E \rangle$ with respect to the number of atoms n which passed through the cavity, (b) shows the evolution of $\langle Y_1 \rangle$ and (c) shows the evolution of $\langle Y_2 \rangle$.

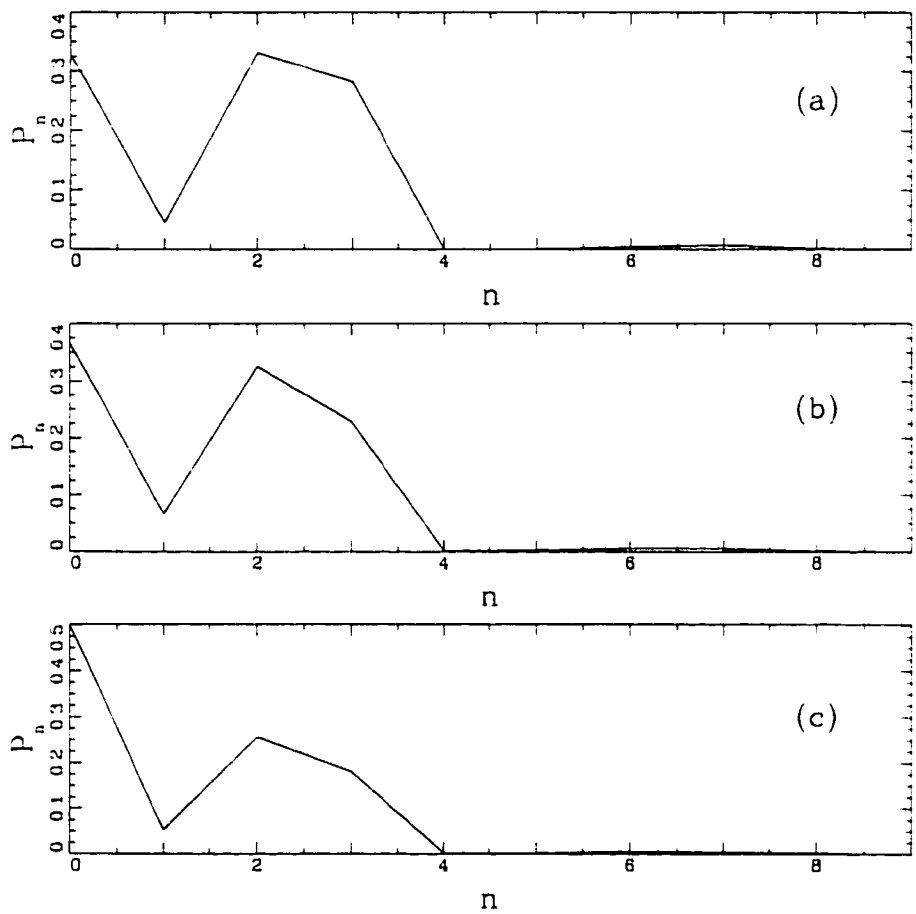

Figure 4.3: Photon number distribution $P_n = \rho_{nn}$ of the cavity field for the initial state (a), after interaction with 20 atoms (b), and after interaction with 100 atoms (c).

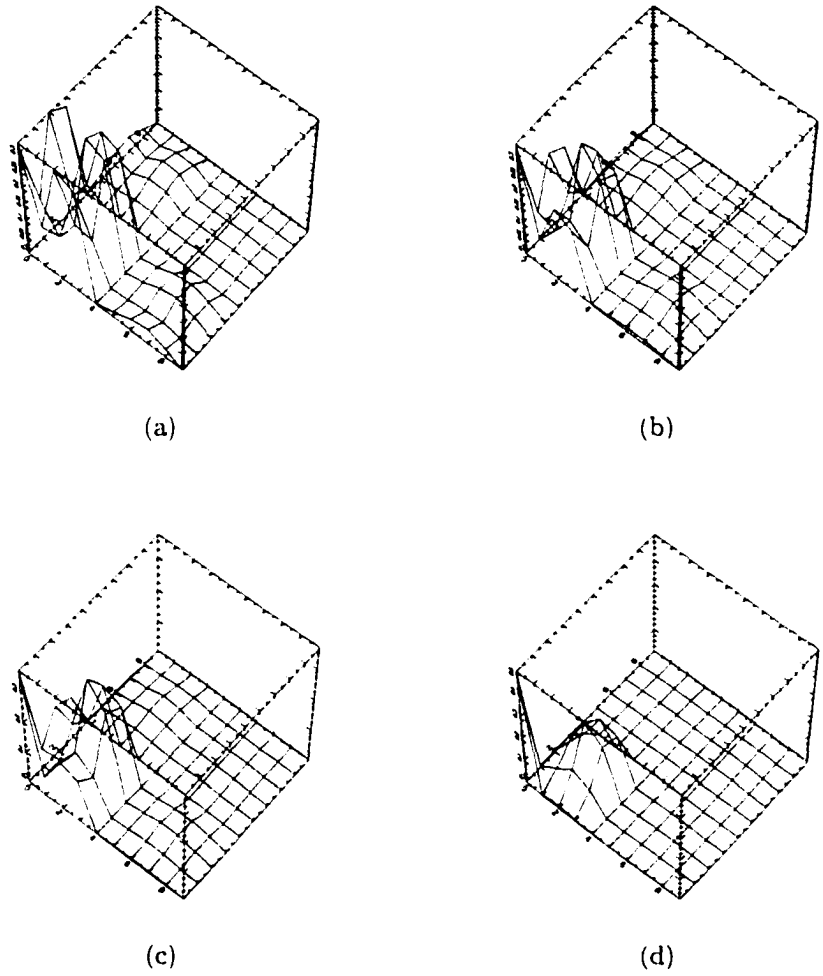

Figure 4.4: Moduli of cavity field density matrix, (a) shows initial state, the nondiagonal peaks are apparent. (b) shows the state after interaction with 10 atoms, (c) after 20 atoms, (d) after 100 atoms.

Chapter 5

Disentanglement-preserving states

5.1 Introduction

The major contribution in the area of micromasers with atoms injected in the superposition of their upper and lower states was made by Slosser et.al. [10. 26, 11]. They found tangent and contangent field states, see Chapter 4. which are preserved when an atom traverses the cavity. In the absence of damping tangent and cotangent states are steady states of the micromaser field. These states can only exist if the micromaser has trapping states which

separate the photon Fock space into noninteracting blocks. It is possible to create period-two steady states by putting tangent and cotangent states in adjacent blocks.

In a somewhat different vein Julio Gea-Banacloche has considered a single two-level atom interacting with a single-mode cavity field, the Jaynes-Cummings model, and found atom-field states which remain approximately in product form for long periods of time [17]. That is, these states, which he called quasiclassical states, are initially products of atom and field states, and, even though the state changes with time, it remains, to good approximation, the product of an atomic and a field state, see Eq. (3.25). The atomic states in the quasiclassical states are, it should be noted, coherent superpositions of the upper and lower states, see Eq. (3.23). Because of their simple time evolution these states are useful in understanding and clarifying the dynamics of the Jaynes-Cummings model. They were used in Section 3.4 for finding the approximate expression for the phase distribution of the steady-state micromaser field, for example.

In this chapter we combine some of the aspects of both of these perspectives. We consider a micromaser cavity with an initial field state and an atom in a coherent superposition state. We are interested in finding field

states which. after interacting with one atom, yield a total atom-field state which is a product. Clearly the tangent and cotangent states are special cases of these states and have the additional property that the field state is unchanged by the passage of the atom. For other states of this type the field state will be different before and after interaction with the atom. One special case, which will be discussed in Section 5.2, is a state which has the sign of the expectation value of its electric field flipped by the atom. Other examples are discussed in Section 5.3.

5.2 Solution causing phase change of the cavity field

The micromaser system during the atom-field interaction is described by the Jaynes-Cummings Hamiltonian as given in Chapter 2, see Eq. (2.1). which gives the time evolution of the total state vector according Eq. (2.18)

$$|f\rangle \otimes (\alpha|a\rangle + \beta|b\rangle) \rightarrow \sum_{n=0}^{\infty} d_n(\alpha c_{n+1}|n\rangle - \mathrm{i}\beta s_n|n-1\rangle) \otimes |a\rangle + \sum_{n=0}^{\infty} d_n(\beta c_n|n\rangle - \mathrm{i}\alpha s_{n+1}|n+1\rangle) \otimes |b\rangle.$$

if the initial state of the atom and the field is described by Eq. (2.16) and Eq. (2.17) respectively. Note that this state is in general an entangled state of the atom and the field. In order for it to be a product the coefficients d_n must satisfy some special conditions.

Rather than find the most general conditions which the d_n should satisfy, let us first look at a special case. Taking a hint from the tangent and cotangent states let us try to find field states which are rotated in phase space by their interaction with the atom (the tangent and cotangent states are rotated by an angle of zero). Note that the effect of such an interaction is to conserve the magnitude of d_n but to change its phase. Therefore, we want to find cavity field states, $|f\rangle$, such that

$$|f\rangle \otimes (\alpha|a\rangle + \beta|b\rangle) \rightarrow \mathrm{e}^{-\mathrm{i}\theta\hat{n}}|f\rangle \otimes (\alpha'|a\rangle + \beta'|b\rangle), \tag{5.1}$$

where $\hat{n}$ denotes the number operator $a^\dagger a$. If we employ Eq. (2.18) on the left hand side of Eq. (5.1) and then equate the coefficients of the vectors $|a\rangle$ and $|b\rangle$ separately, we obtain two reccurence relations for coefficients d_n of the cavity field

$$d_{n+1} = \mathrm{i}\frac{\alpha'\mathrm{e}^{-\mathrm{i}\theta n} - \alpha c_{n+1}}{\beta s_{n+1}} d_n \tag{5.2}$$

$$d_{n+1} = \mathrm{i}\frac{\alpha s_{n+1}}{\beta c_{n+1} - \beta' \mathrm{e}^{-\mathrm{i}\theta(n+1)}} d_n. \tag{5.3}$$

These relations must be the same for any n in order to satisfy Eq. (5.1) which gives in turn

$$\alpha'\beta \mathrm{e}^{-\mathrm{i}\theta n} c_{n+1} - \alpha'\beta' \mathrm{e}^{-\mathrm{i}\theta(2n+1)} + \alpha\beta' \mathrm{e}^{-\mathrm{i}\theta(n+1)} c_{n+1} - \alpha\beta = 0. \tag{5.4}$$

As one can see Eq. (5.4) is fulfilled for any n only if $\theta = 0$ or $\theta = \pi$. Let us take a closer look at the cavity fields in these two cases.

5.2.1 Solutions corresponding to $\theta = 0$.

Substituting $\theta = 0$ into Eq. (5.4) we find

$$\alpha'\beta c_{n+1} - \alpha'\beta' + \alpha\beta' c_{n+1} - \alpha\beta = 0, \tag{5.5}$$

which can be solved for α' and β' in two ways, each providing a different cavity field.

1. The first solution of Eq. (5.5) is $\alpha' = \alpha$ and $\beta' = -\beta$. The reccurence

relations in Eqs. (5.2) and (5.3) then yield the well known tangent state

$$d_{n+1} = \mathrm{i}\frac{\alpha}{\beta}\tan\left(\frac{g\tau\sqrt{n+1}}{2}\right)d_n. \tag{5.6}$$

2. For the second solution we find that $\alpha' = -\alpha$ and $\beta' = \beta$ which after using the reccurence relations gives us the cotangent state

$$d_{n+1} = -\mathrm{i}\frac{\alpha}{\beta}\cot\left(\frac{g\tau\sqrt{n+1}}{2}\right)d_n. \tag{5.7}$$

The cotangent and tangent states have been studied thoroughly and their properties are well understood [12, 10]. We merely note that they can exist only when trapping states are present and the parity of the trapping states determines which of the two kinds of states is physically possible in a given subregion of Fock space. Later we provide a specific example which illustrates the case.

5.2.2 Solutions corresponding to $\theta = \pi$.

Substituting $\theta = \pi$ into Eq. (5.4) we find

$$\alpha'\mathrm{e}^{-\mathrm{i}\pi n}\beta c_{n+1} - \alpha'\beta' + \alpha\beta'\mathrm{e}^{-\mathrm{i}\pi n}c_{n+1} - \alpha\beta = 0 \tag{5.8}$$

which we can again solve in two different ways.

1. If $\alpha' = \alpha$ and $\beta' = \beta$ the reccurence relations give

$$d_{n+1} = \mathrm{i}\frac{\alpha}{\beta}\frac{(-1)^n - c_{n+1}}{s_{n+1}}d_n, \tag{5.9}$$

which takes two different forms depending on the parity of n

i) for even n we have

$$d_{n+1} = \mathrm{i}\frac{\alpha}{\beta}\tan\left(\frac{g\tau\sqrt{n+1}}{2}\right)d_n \tag{5.10}$$

ii) for odd n we get

$$d_{n+1} = -\mathrm{i}\frac{\alpha}{\beta}\cot\left(\frac{g\tau\sqrt{n+1}}{2}\right)d_n. \tag{5.11}$$

2. If $\alpha' = -\alpha$ and $\beta' = -\beta$ we have

$$d_{n+1} = -\mathrm{i}\frac{\alpha}{\beta}\frac{(-1)^n + c_{n+1}}{s_{n+1}}d_n \tag{5.12}$$

which also takes two different forms depending on the parity of n

i) for even n it reads

$$d_{n+1} = -\mathrm{i}\frac{\alpha}{\beta}\cot\left(\frac{g\tau\sqrt{n+1}}{2}\right)d_n \tag{5.13}$$

ii) for odd n it reads

$$d_{n+1} = \mathrm{i}\frac{\alpha}{\beta}\tan\left(\frac{g\tau\sqrt{n+1}}{2}\right)d_n. \tag{5.14}$$

It is clear from the analytic properties of the cotangent and tangent functions that these states are normalizeable only in the presence of trapping states. The position and the parity of the trapping states are crucial in determining the physical existence of the solutions. In particular, if we want the solution to start at $n = 0$, then we find the second solution is ruled out. A close examination reveals that if Eq. (5.1) is satisfied when $\alpha = -\alpha'$, $\beta = -\beta'$, and $n = 0$, then we must have that $-d_0 = c_0 d_0 = d_0$. This implies that $d_0 = 0$, which means that the entire solution vanishes.

The effect of the interaction with an atom on these field states is simply to multiply the field expansion coefficients, d_n, by $(-1)^n$. This has the effect of flipping the sign of the expectation value of any operator, such as the annihilation operator, which only has nonzero matrix elements between

successive number states. In particular, this will happen to the electric field (it is proportional to $a + a^\dagger$). Note that this is true even when the field state has a large number of photons, so that interaction with a single atom could have a macroscopic effect.

Another interesting feature of these solutions shows up if we suppose that the field interacts with atoms which alternate their states between $\alpha|a\rangle + \beta|b\rangle$ and $\alpha|a\rangle - \beta|b\rangle$. Then the field $|f''\rangle$ after two interactions is given by $|f''\rangle = \sum_n (-1)^n d'_n |n\rangle$, where d'_n is the field component left after the first atom. This means that after two atoms the field has returned to its original state, and that the sign of the electric field will flip back and forth as the atoms are injected.

5.3 General solution

Here we shall again seek states of the micromaser which yield output states which can be written as product of field and atomic states,

$$|f\rangle \otimes (\alpha|a\rangle + \beta|b\rangle) \rightarrow |f'\rangle \otimes (\alpha'|a\rangle + \beta'|b\rangle). \tag{5.15}$$

However, we will now not limit ourselves to the special case considered in the previous section, but will seek to find a general solution.

The right hand side of Eq. (5.15) can be expressed using the Eq. (2.18) giving

$$\sum_{n=0}^{\infty} d'_n(\alpha'|a\rangle + \beta'|b\rangle) \otimes |n\rangle = \sum_{n=0}^{\infty} \{(\alpha d_n c_{n+1} - \mathrm{i}\beta d_{n+1} s_{n+1}) \otimes |a\rangle + (\beta d_n c_n - \mathrm{i}\alpha d_{n-1} s_n) \otimes |b\rangle\} |n\rangle. \quad (5.16)$$

This equation will be satisfied if the field state multiplying the atomic state $|a\rangle$ is the same as that multiplying the atomic state $|b\rangle$ up to a constant factor, i. e. if

$$\alpha d_n c_{n+1} - \mathrm{i}\beta d_{n+1} s_{n+1} = z(\beta d_n c_n - \mathrm{i}\alpha d_n s_n), \quad (5.17)$$

where z is a complex number. If there exists a z for which the Eq. (5.17) is satisfied for all n then our objective is met. The values of z can, in fact, be found from the system of linear homogeneous equations which result from Eq. (5.17) for all different values of n. A nontrivial solution for the field components d_n exists only when the determinant of the matrix of the system

is equal to zero

$$\begin{vmatrix} z\beta c_0 - \alpha c_1 & \mathrm{i}\beta s_1 & 0 & 0 & 0 & \dots \\ -\mathrm{i}z\alpha s_1 & z\beta c_1 - \alpha c_2 & \mathrm{i}\beta s_2 & 0 & 0 & \dots \\ 0 & -\mathrm{i}z\alpha s_2 & z\beta c_2 - \alpha c_3 & \mathrm{i}\beta s_3 & 0 & \dots \\ 0 & 0 & -\mathrm{i}z\alpha s_3 & z\beta c_3 - \alpha c_4 & \mathrm{i}\beta s_4 & \dots \\ & & \dots & & & \end{vmatrix} = 0. \quad (5.18)$$

Eq. (5.18) then, determines the values of the variable z. Once z is known it can be substituted into the Eq. (5.17) which can then be used to find the components of the initial cavity field. The most difficult part of the problem is solving Eq. (5.18); it is very hard to find analytical solutions for a general order of the determinant. We shall discuss a simplified case having only a limited number of non-zero field components.

5.4 An example

As an example we chose to have a π trapping state at $|6\rangle$ i.e. the atom-field interaction time τ satisfies $g\tau\sqrt{6} = \pi$, and we limited nonzero field components to those between states $|0\rangle$ and $|5\rangle$. We assumed in our numerical

simulations that $\alpha = 0.8$, $\beta = 0.6$ and $g = 4.40 \times 10^4 Hz$. The trapping condition then implies that $\tau = 2.91 \times 10^{-5} s$. We found the general solutions of which there are six. Among them, two correspond to the case considered in Section 5.2.

We first solved Eq. (5.18) numerically, and then Eq. (5.17) was employed to find the field components $d_0, d_1, \ldots d_5$ for each value of the parameter z. There are six different values of z, two of them yielding cavity fields that were identified as solutions of Eq. (5.1). The first one corresponds to $z_1 = -\alpha/\beta$ and is the cotangent state given by Eq. (5.7). The second corresponds to $z_2 = \alpha/\beta$, and is identical to the state defined by Eq. (5.9). The probability $P_n = d_n^* d_n$ versus photon number, n, of the resulting fields has been plotted in Figure 5.1.

The final field states were also calculated, i.e. we let the initial states interact with one atom during a time interval τ. Probabilities P_n versus n of the cavity field states are shown in Figure 5.2. As one would expect the magnitudes of the two fields corresponding to z_1 and z_2 are left unchanged since only the phase of the field changes according Eq. (5.1). If we compare the fields belonging to $z_3, \ldots, z_6$ to those in Figure 5.1, we see that the interaction with the atom does change these fields. Clearly, the solutions of

Eq. (5.1) are a subset of the more general set which satisfy Eq. (5.15).

5.5 Conclusions

We have studied states of the micromaser field which, upon interaction with one atom yield atom-field states which are disentangled. This means that when the atom leaves the cavity the field is in a pure rather than a mixed state. There is a large set of such states, and we have given a general method for finding them as well several explicit examples.

There are other questions which can be raised in regard to these states. Can one design a sequence of atoms which will cause the micromaser to cycle among these states, always leaving the cavity field in a pure state between atoms? Can one find states which are disentangled after the passage of two atoms?

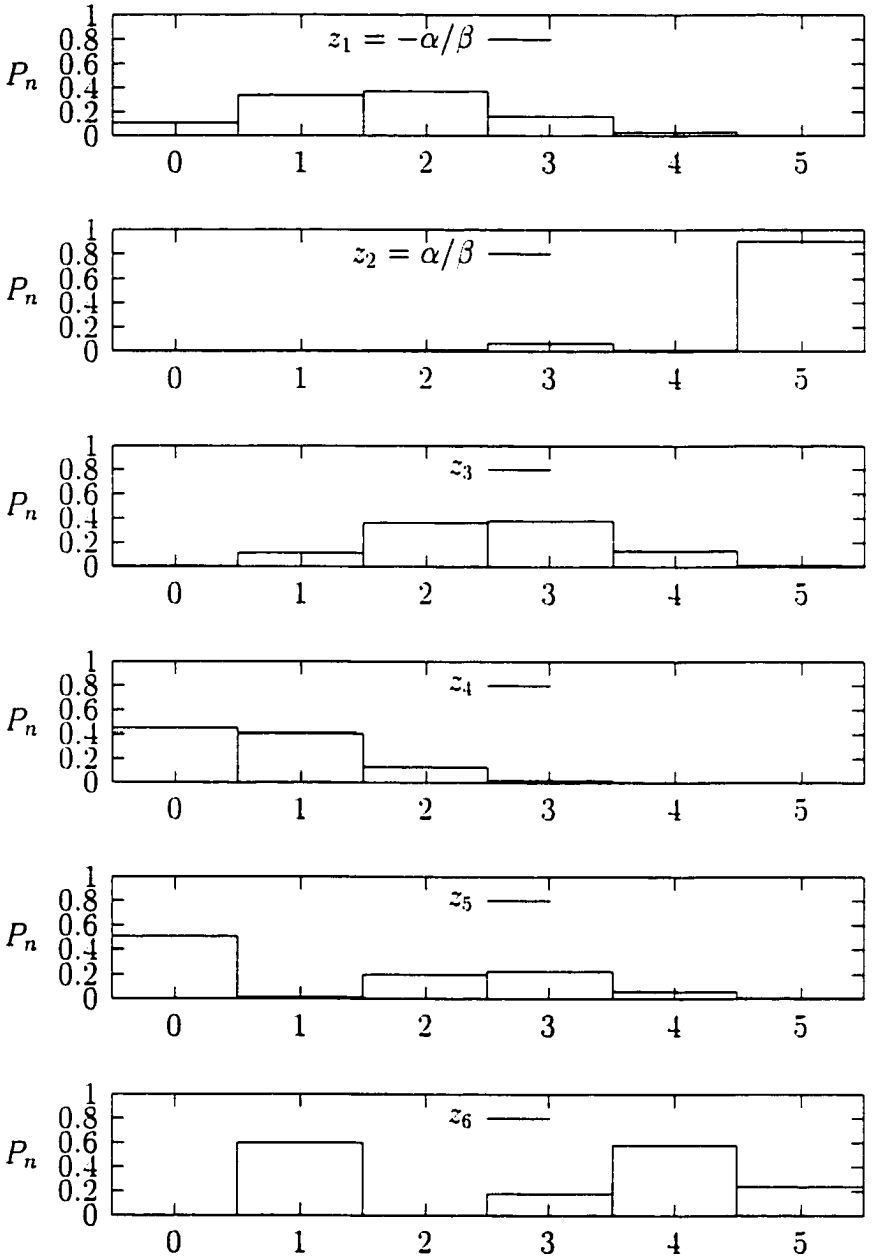

Figure 5.1: Initial states. Probability $P_n = d_n^* d_n$ versus number state n is plotted for the case $\alpha = 0.8$, $\beta = 0.6$ and $g = 4.40 \times 10^4 Hz$ with a π trapping state at $|6\rangle$.

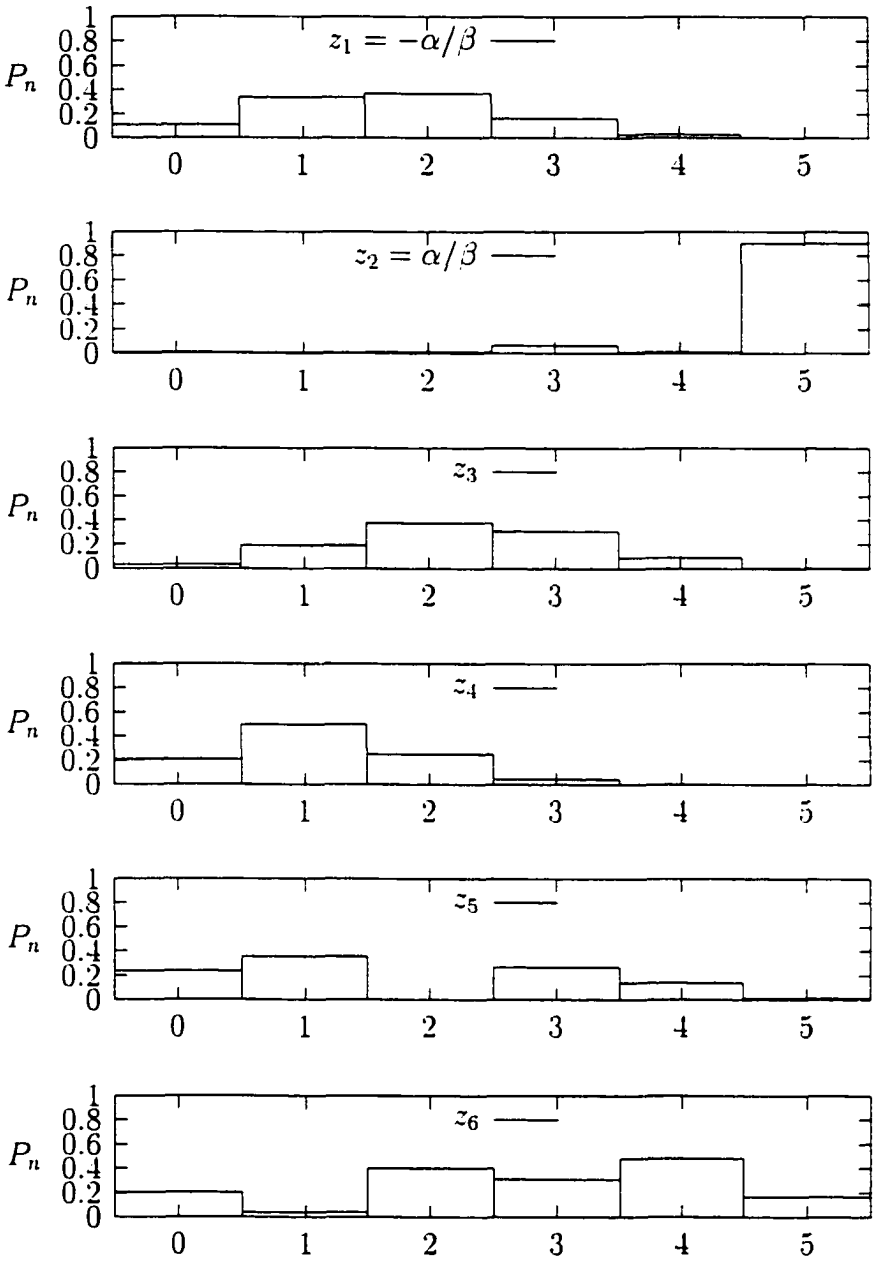

Figure 5.2: Final states. Probability $P_n = d_n^* d_n$ versus number state n is plotted for the same parameters as in Figure 5.1. Both states corresponding to z_1 and z_2 are left unchanged whereas that is not true for the others.

Bibliography

[1] P. Filipowicz, J. Javanainen, and P. Meystre. Theory of microscopic maser. *Physical Review A*, 34(4):3077–3087, October 1986.

[2] P. Filipowicz, J. Javanainen, and P. Meystre. *J. Opt. Soc. Am. B*, 3:906, 1986.

[3] M. Sargent III, M. O. Scully, and W. E. Lamb Jr. *Laser Physics*. Addison-Wesley Publ., London, 1974.

[4] A. M. Guzman, P. Meystre, and E. M. Wright. Semiclassical theory of a micromaser. *Physical Review A*, 40(5):2471–2478, September 1989.

[5] D. Meschede, H. Walther, and G. Muller. One-atom maser. *Physical Review Letters*, 54(6):551–554, February 1985.

[6] G. Rempe, F. Schmidt-Kaler, and H. Walther. Observation of sub-Poissonian photon statistics in a micromaser. *Physical Review Letters*, 64(23):2783–2786, June 1990.

[7] M. Brune, F. Schmidt-Kaler, A. Maali, J. Dreyer, E. Hagley, J. M. Raimond, and S. Haroche. Quantum Rabi oscillation: A direct test of field quantization in a cavity. *Physical Review Letters*, 76(11):1800–1803, March 1996.

[8] G. Rempe, H. Walther, and N. Klein. Observation of quantum collapse and revival in a one-atom maser. *Physical Review Letters*, 58(4):353–356, January 1987.

[9] J. Krause, M. O. Scully, and H. Walther. Quantum theory of a micromaser: Symmetry breaking via off-diagonal atomic injection. *Physical Review A*, 34(3):2032–2037, September 1986.

[10] J. J. Slosser and P. Meystre. Tangent and cotangent states of the electromagnetic field. *Physical Review A*, 41(7):3867–3874, April 1990.

[11] J. Slosser, P. Meystre, and E. Wright. Generation of macroscopic superpositions in a micromaser. *Opt. Lett.*, 15:233–235, February 1990.

[12] J. J. Slosser, P. Meystre, and S. L. Braunstein. *Physical Review Letters*, 63:934–, 1989.

[13] F. L. Kien, G. M. Meyer, U. W. Rathe, M. O. Scully, H. Walther, and S. Zhu. Two-mode Λ laser with atoms injected in a superposition of their states. *Physical Review A*, 52(4):3279–3298, October 1995.

[14] W. H. Louisell. *Quantum Statistical Properties of Radiation*. John Wiley and Sons, New York, 1973.

[15] C. Benkert, M. O. Scully, J. Bergou, L. Davidovich, M. Hillery, and M. Orszag. Role of pumping statistics in laser dynamics: Quantum Langevin approach. *Physical Review A*, 41(5):2756–2765, March 1990.

[16] U. Herzog and J. A. Bergou. Non-Markovian dynamics of the micromaser due to discrete and continuous non-Poissonian pumping. *Physical Review A*, 54(6):5334–5344, December 1996.

[17] J. Gea-Banacloche. Atom- and field-state evolution in the Jaynes-Cummings model for large initial fields. *Physical Review A*, 44(9):5913–5931, November 1991.

[18] D. F. Walls and G. J. Milburn. *Quantum Optics*. Springer, Berlin, 2nd edition, 1995.

[19] L. Mandel and E. Wolf. *Optical Coherence and Quantum Optics*. Cambridge Univ. Press, New York, 1995.

[20] J. A. Bergou, M. Hillery, and P. Bogar. *to be published.*

[21] J. Bergou, L. Davidovich, M. Orszag, C. Benkert, M. Hillery, and M. O. Scully. *Opt. Commun.*, 72:82, 1989.

[22] F. Haake, S. M. Tan, and D. F. Walls. Photon noise reduction in lasers. *Physical Review A*, 40(12):7121–7132, December 1989.

[23] M. A. M. Marte and P. Zoller. Laser with sub-poissonian pump. *Physical Review A*, 40(10):5774–5782, November 1989.

[24] H. Briegel, B. Englert, and M. O. Scully. Spectral properties of a micromaser: Atomic-beam statistics and the field correlation function. *Physical Review A*, 54(4):3603–3613, October 1996.

[25] U. Herzog and J. Bergou. Reflection of the Jaynes-Cummings dynamics in the spectrum of a regularly pumped micromaser. *Physical Review A*, 55(2):1385–1390, February 1997.

[26] M. Hillery and J. Skvarcek. Field oscillations in a micromaser with injected atomic coherence. *Journal of Modern Optics*, 45(8):1717–1724, 1998.